Title

Two-Dimensional Electronic–Vibrational Spectroscopy Reveals Cross-Correlation between Solvation Dynamics and Vibrational Spectral Diffusion

Journal

The Journal of Physical Chemistry B, 124(49)

ISSN

1520-6106

Authors

Cho, Minhaeng
Fleming, Graham R

Publication Date

2020-12-10

DOI

10.1021/acs.jpcb.0c08959

Peer reviewed

THE JOURNAL OF PHYSICAL CHEMISTRY B

pubs.acs.org/JPCB Article

Two-Dimensional Electronic–Vibrational Spectroscopy Reveals Cross-Correlation between Solvation Dynamics and Vibrational Spectral Diffusion

Published as part of The Journal of Physical Chemistry virtual special issue "Yoshitaka Tanimura Festschrift".

Minhaeng Cho* and Graham R. Fleming

Cite This: *J. Phys. Chem. B* 2020, 124, 11222–11235 Read Online

ACCESS | Metrics & More | Article Recommendations

ABSTRACT: Two-dimensional electronic–vibrational spectroscopy (2DEVS) is a useful technique for studying the structure and dynamics of photoexcited molecules via monitoring of the vibrational spectrum in real-time. However, quantitative modeling or prediction of experimental spectra has been hampered by the lack of a firm theoretical basis for this quantity. Here, we develop a useful theory of 2DEVS and show that the time-dependent line shape of the 2DEVS spectrum provides invaluable information on the cross-correlation function of the solvation dynamics and vibrational spectral diffusion. The center and nodal line slopes of each 2DEVS peak are determined by the associated cross-electronic–vibrational frequency–frequency correlation function, which is shown to be related to the intermolecular interactions and vibrational anharmonicities. The present theory of 2DEVS would thus be of use for a refined understanding of the 2DEVS spectra of reactive chemical and biological systems. We anticipate that further development of the expressions developed here will illuminate the application of 2DEVS studies of vibronically induced energy and electron transfer in functional materials.

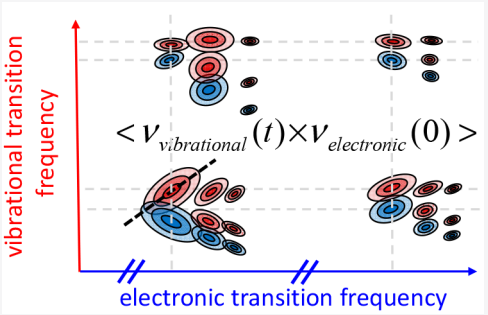

INTRODUCTION

Four-wave-mixing spectroscopy, including pump–probe and 2D electronic spectroscopy (2DES) or IR spectroscopy, has been used extensively to investigate chemical and physical processes of molecules and biological systems in condensed phases.[1−3] One of the most successful approaches is 2DES,[4−6] which enables one to measure the time-correlation of electronic transition frequencies reflecting changes in the chemical structure or conformation of a given chromophore in solution.[7] 2D IR (Raman) spectroscopy[8,9] is a vibrational analog of 2DES, which has also been used as an incisive technique for extracting information on the dynamics and structure of either a molecule in a thermal equilibrium state or one in a nonequilibrium state generated by an external perturbation, e.g., temperature, pressure, pH jump, or photoexcitation.[2,10−14]

An exciting development in the 2DIR research community is the site-specific incorporation of vibrational probes into molecular, biological, or functional material systems using a variety of organic and biochemical techniques.[15] Although such an IR probe could be invasive when it is incorporated into a solvated molecular system via its hydrogen-bonding interactions with surrounding solvent molecules or biomolecular residues, the perturbation induced by the IR probe is often negligibly weak compared to bulky organic fluorophores or fluorescent proteins. The IR-probe-labeled biomolecules, materials, and reactive systems have thus been under extensive investigation using various time-resolved vibrational spectroscopic methods. Rigorous and systematic theoretical approaches, which are capable of describing the vibrational solvatochromism, vibrational electrochromism, or the Stark effect and dynamic fluctuations of vibrational frequencies and transition dipole moments affected by surrounding solvent molecules or neighboring residues in proteins and nucleic acids, have only recently been developed and begun to be used in the quantitative interpretation of time-resolved vibrational spectroscopy signals.[16]

Recently, 2D electronic–vibrational spectroscopy (2DEVS),[17] which is another four-wave-mixing technique utilizing both visible (or near-IR) and IR pulses, has been shown to be of exceptional use for studying the chemical dynamics of electronically excited molecules via probing the time-dependent changes in vibrational structure through

Received: October 1, 2020
Revised: November 10, 2020
Published: November 30, 2020

https://dx.doi.org/10.1021/acs.jpcb.0c08959
J. Phys. Chem. B 2020, 124, 11222–11235

measuring time-resolved IR spectroscopic signals. In the 2DEVS experiment, the first two pulses propagating along the same direction are pump fields in the visible frequency domain. The third pulse in the IR region interacts with the excited molecules to create third-order polarization. Then, the pump−probe-type 2DEVS signal field is interferometrically detected by a local oscillator pulse in the IR region. With the 2DEVS, one can directly measure the correlated inhomogeneity of the fluctuating energy gaps between electronic states and vibrational states by analyzing a 2DEV spectrum that is time-resolved by the waiting time between the visible (or near-IR) pump pulse and the IR probe pulse.[18] For example, the application of 2DEVS in revealing vibronic coupling has been explored.[19,20] However, the origin of the cross-correlation between fluctuating electronic and vibrational energy gaps has not yet been clearly elucidated. One of the 2DEV spectroscopic observables is the center line slope (CLS) of a given 2DEVS peak, which has been extensively used for qualitatively interpreting the 2DEV spectra of a number of photochemical systems. However, quantitative modeling or prediction of experimental spectra has been hampered by the lack of a firm theoretical basis for this quantity. This paper aims to provide such a foundation and to give simplified expressions that make intuitively clear the physical origin of the 2DEVS dynamics. This framework should allow for a refined understanding of 2DEV spectra of systems such as those undergoing a sudden change in electronic structure as a result of passing through a conical intersection[21,22] or a keto-to-enol transition leading to a conical intersection.[23]

In the present work, we first develop a theory of 2DEVS by invoking a short-time approximation[2,24] to the associated nonlinear response function. It is then shown that the time-dependent line shape of each 2DEV spectrum can be directly related to the cross-correlation function of the fluctuating parts of the electronic energy gap and vibrational energy gap of a given chromophore in a condensed phase, which are induced by the chromophore−solvent interactions and dynamics. Further elaboration of the expressions developed here will illuminate the application of 2DEVS studies of vibronically induced energy[25,26] and electron transfer.

RESULTS AND DISCUSSION

Molecular Hamiltonian. In general, the three radiation−matter interactions can induce quantum transitions among four different stationary states, including the initial ground state $|g\rangle$. We shall therefore consider a four-level-system as a model for third-order response spectroscopy.[27,28] The four-level-system Hamiltonian is

$$\hat{H}_{4LS} = |a\rangle\hbar\omega_{ag}\langle a| + |b\rangle\hbar\omega_{bg}\langle b| + |c\rangle\hbar\omega_{cg}\langle c| \tag{1}$$

where the energy of the ground state E_g is assumed to be zero. The three ket states $|a\rangle$, $|b\rangle$, and $|c\rangle$ represent any vibrationally excited states on the electronic ground state or vibrational states on the electronically excited state. Due to the system−bath interaction, the energy gaps fluctuate in time, which can be approximately described by the following Hamiltonian that includes the bath and the system−bath interaction

$$\hat{H}_{mol} = \hat{H}_{4LS} + \hat{H}_B + \hat{H}_{SB} \tag{2}$$

The system−bath (chromophore−solvent) interaction Hamiltonian,[29] denoted as $\hat{H}_{SB}$, is assumed to be diagonal with respect to the system eigenstates as

$$\hat{H}_{SB} = V_{ag}(\mathbf{q})|a\rangle\langle a| + V_{bg}(\mathbf{q})|b\rangle\langle b| + V_{cg}(\mathbf{q})|c\rangle\langle c| \tag{3}$$

The bath degrees of freedom are denoted as $\mathbf{q}$, and the potential energy differences that are parametrically dependent on $\mathbf{q}$ are defined as $V_{jg}(\mathbf{q}) = V_j(\mathbf{q}) - V_g(\mathbf{q})$ for $j = a$, b, and c. Therefore, we have

$$\begin{aligned}\hat{H}_{mol} &= \sum_{m=g,a,b,c} \{\hbar\omega_m + V_m(\mathbf{q}) + H_B(\mathbf{q})\}|m\rangle\langle m| \\ &= \hat{H}_0 + \hat{H}'\end{aligned} \tag{4}$$

where

$$\begin{aligned}\hat{H}_0 &= \{\hbar\omega_g + V_g(\mathbf{q}) + H_B(\mathbf{q})\} \sum_{m=g,a,b,c} |m\rangle\langle m| \\ \hat{H}' &= \sum_{m=a,b,c} \{\hbar\omega_{mg} + V_{mg}(\mathbf{q})\}|m\rangle\langle m|\end{aligned} \tag{5}$$

The ground-state adiabatic Hamiltonian $\hat{H}_g(\mathbf{q})$, defined as $\hat{H}_g(\mathbf{q}) = \hbar\omega_g + V_g(\mathbf{q}) + H_B(\mathbf{q})$, is the reference Hamiltonian, so $\hat{H}_j(\mathbf{q})$ (for $j = a$, b, and c) can be written as

$$\hat{H}_j(\mathbf{q}) = \hat{H}_g(\mathbf{q}) + \hbar\omega_{jg} + V_{jg}(\mathbf{q}) \tag{6}$$

Treating $\hat{H}_g(\mathbf{q})$ as the zero-order Hamiltonian $\hat{H}_0$, we find that in the interaction picture the forward and backward time-evolution operators entirely determined by $\hat{H}_j(\mathbf{q})$ (for $j = a$, b, and c) are

$$\begin{aligned}\exp\left(-\frac{i}{\hbar}\hat{H}_j t\right) &= \exp(-i\bar{\omega}_{jg}t)\exp\left(-\frac{i}{\hbar}\hat{H}_g t\right)\exp_+\left(-\frac{i}{\hbar}\int_0^t d\tau\, U_{jg}(\tau)\right) \\ \exp\left(\frac{i}{\hbar}\hat{H}_j t\right) &= \exp(i\bar{\omega}_{jg}t)\exp_-\left(\frac{i}{\hbar}\int_0^t d\tau\, U_{jg}(\tau)\right)\exp\left(\frac{i}{\hbar}\hat{H}_g t\right)\end{aligned} \tag{7}$$

where

$$\begin{aligned}\bar{\omega}_{jg} &= \omega_{jg} + \hbar^{-1}\langle V_{jg}(\mathbf{q})\rangle \\ U_{jg}(\mathbf{q}) &\equiv V_{jg}(\mathbf{q}) - \langle V_{jg}(\mathbf{q})\rangle \\ U_{jg}(t) &= U_{jg}(\mathbf{q}(t)) = \exp\left(\frac{i}{\hbar}\hat{H}_B t\right) U_{jg}(\mathbf{q}) \exp\left(-\frac{i}{\hbar}\hat{H}_B t\right)\end{aligned} \tag{8}$$

The initial density operator may be written as a product of the system and bath density operators as $\rho(-\infty) = \rho_S(-\infty)\rho_B(-\infty)$. In eq 8, $\langle\ldots\rangle$ represents the average over the bath degrees of freedom.

Field−Matter Interaction Hamiltonian and Third-Order Response Function. The third-order spectroscopy involves three field−matter interactions.[1] In the 2DEVS, all the field−matter interactions within the electric dipole approximation are given by

$$\hat{H}_{Int}(\mathbf{r}, t) = -\sum_{j=1}^{3} \hat{\boldsymbol{\mu}}\cdot\mathbf{E}_j(\mathbf{r}, t) \tag{9}$$

Here, $E_j(\mathbf{r}, t) = \boldsymbol{E}_j(t)\exp(i\mathbf{k}_j\mathbf{r} - i\omega_j t) + c.c.$, where $\boldsymbol{E}_j(t)$, $\mathbf{k}_j$, and ω_j are the temporal envelope function, wave vector, and carrier angular frequency of the jth field, respectively, and $c.c.$ is the complex conjugate. Using the third-order time-dependent perturbation theory, one can write the macroscopic third-order (in the external field) polarization, which is proportional to the expectation value of an electric dipole operator, in terms of nonlinear response function and convolution integrals:[1,2,29,30]

https://dx.doi.org/10.1021/acs.jpcb.0c08959
J. Phys. Chem. B 2020, 124, 11222−11235

$$\boldsymbol{P}^{(3)}(\mathbf{r}, t) = N\langle\hat{\boldsymbol{\mu}}\rho^{(3)}(\mathbf{r}, t)\rangle = \left(\frac{i}{\hbar}\right)^3 \int_{t_0}^{t} \mathrm{d}\tau_3 \int_{t_0}^{\tau_3} \mathrm{d}\tau_2 \int_{t_0}^{\tau_2} \mathrm{d}\tau_1 \langle[[[\hat{\boldsymbol{\mu}}(t), \hat{\boldsymbol{\mu}}(\tau_3)], \hat{\boldsymbol{\mu}}(\tau_2)], \hat{\boldsymbol{\mu}}(\tau_1)]\, \rho(t_0)\rangle \vdots \boldsymbol{E}_3(\mathbf{r}, \tau_3)\, \boldsymbol{E}_2(\mathbf{r}, \tau_2)\, \boldsymbol{E}_1(\mathbf{r}, \tau_1) \quad (10)$$

where N is the number of chromophores and $\hat{\boldsymbol{\mu}}(t)$ is the time-dependent dipole operator in the interaction picture. Changing the integration variables in eq 10 and assuming that $t_0 = -\infty$, we find that

$$\boldsymbol{P}^{(3)}(\mathbf{r}, t) = \int_0^\infty \mathrm{d}t_3 \int_0^\infty \mathrm{d}t_2 \int_0^\infty \mathrm{d}t_1\, \mathbf{R}(t_3, t_2, t_1) \vdots \boldsymbol{E}_3(\mathbf{r}, t - t_3)\, \boldsymbol{E}_2(\mathbf{r}, t - t_3 - t_2)\, \boldsymbol{E}_1(\mathbf{r}, t - t_3 - t_2 - t_1) \quad (11)$$

where the third-order response function is defined as

$$\mathbf{R}(t_3, t_2, t_1) = \left(\frac{i}{\hbar}\right)^3 \theta(t_3)\, \theta(t_2)\, \theta(t_1) \langle[[[\hat{\mu}(t_3 + t_2 + t_1), \hat{\mu}(t_2 + t_1)], \hat{\mu}(t_1)], \hat{\mu}(0)]\, \rho(-\infty)\rangle \quad (12)$$

The third-order response function of each molecule, which is a fourth-rank tensor, describes the average dipole moment of the molecule at a time of $t_1 + t_2 + t_3$, which interacted with the three applied fields $\mathbf{E}_j$ at $t = 0$, t_1, and $t_1 + t_2$.

Expanding the three commutators in the definition of third-order response function in eq 12, one can find that the nonlinear response function consists of eight different terms:

$$\mathbf{R}(t_3, t_2, t_1) = \left(\frac{i}{\hbar}\right)^3 \theta(t_3)\, \theta(t_2)\, \theta(t_1) \sum_{\alpha=1}^{4} [\mathbf{R}_\alpha(t_3, t_2, t_1) - \mathbf{R}_\alpha^*(t_3, t_2, t_1)] \quad (13)$$

where $\theta(t)$ is the Heaviside step function and

$$\begin{aligned}
\mathbf{R}_1(t_3, t_2, t_1) &\equiv \langle\hat{\mu}(t_1)\, \hat{\mu}(t_1 + t_2)\, \hat{\mu}(t_1 + t_2 + t_3)\, \hat{\mu}(0)\, \rho(-\infty)\rangle \\
\mathbf{R}_2(t_3, t_2, t_1) &\equiv \langle\hat{\mu}(0)\, \hat{\mu}(t_1 + t_2)\, \hat{\mu}(t_1 + t_2 + t_3)\, \hat{\mu}(t_1)\, \rho(-\infty)\rangle \\
\mathbf{R}_3(t_3, t_2, t_1) &\equiv \langle\hat{\mu}(0)\, \hat{\mu}(t_1)\, \hat{\mu}(t_1 + t_2 + t_3)\, \hat{\mu}(t_1 + t_2)\, \rho(-\infty)\rangle \\
\mathbf{R}_4(t_3, t_2, t_1) &\equiv \langle\hat{\mu}(t_1 + t_2 + t_3)\, \hat{\mu}(t_1 + t_2)\, \hat{\mu}(t_1)\, \hat{\mu}(0)\, \rho(-\infty)\rangle
\end{aligned} \quad (14)$$

The double-sided Feynman diagrams corresponding to the four nonlinear response function components are shown in Figure 1. From the definition of time-dependent dipole operator in the interaction picture and using the operator identities in eq 7, one can rewrite the four terms in eq 14 as

$$\begin{aligned}
\mathbf{R}_1(t_3, t_2, t_1) &= \sum_{abc} \mu_{gc}\mu_{cb}\mu_{ba}\mu_{ag} \exp\{-i\bar{\omega}_{ab}t_3 - i\bar{\omega}_{ac}t_2 - i\bar{\omega}_{ag}t_1\}\, F_1(t_3, t_2, t_1) \\
\mathbf{R}_2(t_3, t_2, t_1) &= \sum_{abc} \mu_{gc}\mu_{cb}\mu_{ba}\mu_{ag} \exp\{-i\bar{\omega}_{ab}t_3 - i\bar{\omega}_{ac}t_2 - i\bar{\omega}_{gc}t_1\}\, F_2(t_3, t_2, t_1) \\
\mathbf{R}_3(t_3, t_2, t_1) &= \sum_{abc} \mu_{gc}\mu_{cb}\mu_{ba}\mu_{ag} \exp\{-i\bar{\omega}_{ab}t_3 - i\bar{\omega}_{gb}t_2 - i\bar{\omega}_{gc}t_1\}\, F_3(t_3, t_2, t_1) \\
\mathbf{R}_4(t_3, t_2, t_1) &= \sum_{abc} \mu_{gc}\mu_{cb}\mu_{ba}\mu_{ag} \exp\{-i\bar{\omega}_{cg}t_3 - i\bar{\omega}_{bg}t_2 - i\bar{\omega}_{ag}t_1\}\, F_4(t_3, t_2, t_1)
\end{aligned} \quad (15)$$

Using the Cumulant expansion method,[1] one can obtain the approximate line shape functions $F_j(t_3, t_2, t_1)$.

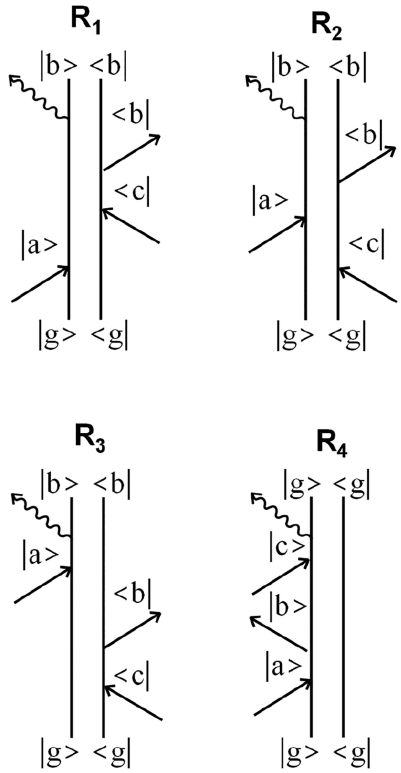

Figure 1. Double-sided Feynman diagrams that are associated with the four response function components in eq 14.

$$\begin{aligned}
F_1(t_3, t_2, t_1) &= \exp\{-g_{cc}^*(t_2) - g_{bb}^*(t_3) - g_{aa}(t_1 + t_2 + t_3) - g_{cb}^*(t_2 + t_3) + g_{cb}^*(t_2) + g_{cb}^*(t_3) + g_{ca}(t_1 + t_2) - g_{ca}(t_1) + g_{ca}^*(t_2 + t_3) - g_{ca}^*(t_3) + g_{ba}(t_1 + t_2 + t_3) - g_{ba}(t_1 + t_2) + g_{ba}^*(t_3)\} \\
F_2(t_3, t_2, t_1) &= \exp\{-g_{cc}^*(t_1 + t_2) - g_{bb}^*(t_3) - g_{aa}(t_2 + t_3) - g_{cb}^*(t_1 + t_2 + t_3) + g_{cb}^*(t_1 + t_2) + g_{cb}^*(t_3) + g_{ca}(t_2) + g_{ca}^*(t_1 + t_2 + t_3) - g_{ca}^*(t_1) - g_{ca}^*(t_3) + g_{ba}(t_2 + t_3) - g_{ba}(t_2) + g_{ba}^*(t_3)\} \\
F_3(t_3, t_2, t_1) &= \exp\{-g_{cc}^*(t_1) - g_{bb}^*(t_2 + t_3) - g_{aa}(t_3) - g_{cb}^*(t_1 + t_2 + t_3) + g_{cb}^*(t_1) + g_{cb}^*(t_2 + t_3) + g_{ca}^*(t_1 + t_2 + t_3) - g_{ca}^*(t_1 + t_2) - g_{ca}^*(t_2 + t_3) + g_{ca}^*(t_2) + g_{ba}(t_3)g_{ba}^*(t_2) + (t_3) - g_{ba}^*(t_2)\} \\
F_4(t_3, t_2, t_1) &= \exp\{-g_{cc}(t_3) - g_{bb}(t_2) - g_{aa}(t_1) - g_{cb}(t_2 + t_3) + g_{cb}(t_2) + g_{cb}(t_3) - g_{ca}(t_1 + t_2 + t_3) + g_{ca}(t_1 + t_2) + g_{ca}(t_2 + t_3) - g_{ca}(t_2) - g_{ba}(t_1 + t_2) + g_{ba}(t_1) + g_{ba}(t_2)\}
\end{aligned} \quad (16)$$

Here, the line-broadening function $g(t)$ is given as

$$g_{xy}(t) = \int_0^t \mathrm{d}\tau_1 \int_0^{\tau_1} \mathrm{d}\tau_2\, C_{xy}(\tau_2) \quad (17)$$

where the frequency−frequency correlation function (FFCF) is

$$C_{xy}(t) = \frac{1}{\hbar^2}\langle U_{xg}(t)\, U_{yg}(0)\rangle = \langle\delta\omega_{xg}(t)\, \delta\omega_{yg}(0)\rangle \quad (18)$$

https://dx.doi.org/10.1021/acs.jpcb.0c08959
J. Phys. Chem. B 2020, 124, 11222−11235

Note that the above quantum mechanical time-correlation function $C_{xy}(t)$ is a complex function of time, and its real and imaginary parts are related to each other via a quantum mechanical fluctuation−dissipation theorem. The fluctuation of the electronic or vibrational transition frequency, induced by the system−bath interaction, is responsible for the dephasing of associated electronic or vibrational coherence created by the interaction between an ensemble of chromophores and ultrashort laser pulses.[31]

Although the third-order response function in eq 15 is exact in the case when the distribution of difference potential V_{jg} (or fluctuating part of the transition frequencies U_{jg}) is a Gaussian function, the calculation of the 2DEVS signal with eq 11 requires complicated convolution integrals. It is not difficult to carry out the integrations numerically. Still, the results may not be useful for understanding the underlying physics nor for interpreting the experimentally measured signals in terms of the dephasing constants, inhomogeneous widths, spectral diffusion, and the time-correlation between two different transition frequency fluctuations. Therefore, it is helpful to obtain approximate expressions for the third-order response functions, which still contain most of the salient features about how chromophore-solvent dynamics affect the time-evolution of the 2DEV spectrum.

Short-Time Approximated Nonlinear Response Function. This short-time approximation to the nonlinear response function is often valid because the electronic or vibrational coherence of the system evolving for the first and third time periods, t_1 and t_3, loses its phase rapidly due to the broad distributions of instantaneous transition frequencies. That is to say, only the short time (slowly varying) parts of the third-order response over the times t_1 and t_3 are essential and sufficient to approximately describe the dephasing processes.[32,33] Mathematically, this is the stationary-phase approximation or the Laplace approximation for an integral of the function multiplied by a highly oscillating function. Taking a 2D Taylor expansion of the exponents in eqs 16 for t_1 and t_3, the 3D line shape function can be recast in the following form.[2]

$$F_j(t_3, t_2, t_1) = \exp\left\{ f_j(t_2) - \frac{1}{2}\delta_j^2(t_2)\, t_1^2 - \frac{1}{2}\Delta_j^2(t_2)\, t_3^2 + H_j(t_2)\, t_1 t_3 - iQ_j(t_2)\, t_3 \right\} \tag{19}$$

Here, $f_j(t_2)$ describes the dephasing of the quantum coherences or populations during t_2 period, and, for j = 1−4, they are

$$\begin{aligned} f_1(t_2) &= f_2(t_2) \\ &= -g_{cc}^*(t_2) - g_{aa}(t_2) + 2Re[g_{ca}(t_2)] \\ f_3(t_2) &= -g_{bb}^*(t_2) \\ f_4(t_2) &= -g_{bb}(t_2) \end{aligned} \tag{20}$$

The t_2-dependent $\delta_j^2(t_2)$ in eq 19 represents the mean square fluctuation amplitude of the transition frequency, which determines the first coherence oscillation over t_1. Note that within the impulsive pulse approximation, $\delta_j^2(t_2)$ determines the spectral bandwidth of the 2D spectrum along with the first frequency (ω_{t_1}) that is the conjugate frequency of t_1. For j = 1−4, we have

$$\begin{aligned} \delta_1^2(t_2) &= C_{ca}(0) + Re[C_{aa}(t_2) - C_{ca}(t_2)] \\ \delta_2^2(t_2) &= C_{ca}(0) - Re[C_{ca}(t_2) - C_{cc}^*(t_2)] \\ \delta_3^2(t_2) &= C_{cc}(0) - C_{cb}(0) + Re[C_{cb}(t_2)] \\ \delta_4^2(t_2) &= C_{aa}(0) - C_{ba}(0) + Re[C_{ba}(t_2)] \end{aligned} \tag{21}$$

Similarly, $\Delta_j^2(t_2)$ in eq 19 is the mean square frequency fluctuation determining the bandwidth of the 2D spectrum along with the frequency (ω_{t_3}) that is the conjugate frequency of t_3, and they are

$$\begin{aligned} \Delta_1^2(t_2) = \Delta_2^2(t_2) &= C_{bb}(0) - C_{cb}(0) - C_{ba}(0) + C_{ca}(0) \\ &\quad + Re[C_{aa}(t_2) + C_{cb}(t_2) - C_{ca}(t_2) - C_{ba}(t_2)] \\ \Delta_3^2(t_2) &= C_{aa}(0) - C_{ba}(0) + Re[C_{bb}(t_2) - C_{ba}(t_2)] \\ \Delta_4^2(t_2) &= C_{cc}(0) - C_{cb}(0) + Re[C_{cb}(t_2)] \end{aligned} \tag{22}$$

The fourth term in the exponent of eq 19, $H_j(t_2)$, describes how the excitation and detection (emission) frequencies are temporally correlated with each other. For j = 1−4, we have

$$\begin{aligned} H_1(t_2) &= Re[C_{ba}(t_2) - C_{aa}(t_2)] \\ H_2(t_2) &= -Re[C_{cb}(t_2) - C_{ca}(t_2)] \\ H_3(t_2) &= -Re[C_{cb}(t_2) - C_{ca}(t_2)] \\ H_4(t_2) &= -Re[C_{ca}(t_2)] \end{aligned} \tag{23}$$

The last term in eq 19, $Q_j(t_2)$, describes spectral diffusion, which is related to the Stokes shift of the transition frequency due to solvation dynamics, during the second period t_2. $Q_j(t_2)$ are

$$\begin{aligned} Q_1(t_2) = Q_2(t_2) &= -Im[\bar{C}_{aa}(t_2) - \bar{C}_{cb}(-t_2) \\ &\quad + \bar{C}_{ca}(-t_2) - \bar{C}_{ba}(t_2)] \\ Q_3(t_2) &= -Im[\bar{C}_{bb}^*(t_2) + \bar{C}_{ba}(-t_2)] \\ Q_4(t_2) &= -Im[\bar{C}_{cb}(t_2)] \end{aligned} \tag{24}$$

In eq 24, for x, y = a, b, and c, the auxiliary function $\bar{C}(t)$ is defined as

$$\bar{C}_{xy}(t) = \int_0^t d\tau\, C_{xy}(\tau) \tag{25}$$

Within this short-time approximation, each line shape function, $F_j(t_3, t_2, t_1)$, is in the form of a rotated Gaussian function with respect to t_1 and t_3, where the 2D widths and the angle of rotation change in time t_2.

2D Electronic−Vibrational Spectroscopy. 2DEVS involves the first two interactions of chromophores with visible pulses separated by τ in the time domain, and the third field−matter interaction is with an IR pulse that is delayed by T from the second pulse. The corresponding wavevectors can be generally denoted as $\mathbf{k}_1$(vis), $\mathbf{k}_2$(vis), and $\mathbf{k}_3$(IR), respectively. In practice, the first two visible pulses are generated by a single pulse with a pulse shaper so that they propagate along the same direction, i.e., $\mathbf{k}_{vis} = \mathbf{k}_1(vis) = \mathbf{k}_2(vis)$, which is known as the pump−probe geometry for coherent 2D spectroscopy.[34,35] Thus, the created third-order polarization in the material produces electromagnetic fields, and the corresponding phase-

https://dx.doi.org/10.1021/acs.jpcb.0c08959
J. Phys. Chem. B 2020, 124, 11222−11235

matching conditions determine their frequencies and propagation directions, i.e., wavevectors. In the present work, we focus on the pump−probe-type 2DEVS so that the polarization component satisfying the following phase-matching requirement, $\mathbf{k}_s = -\mathbf{k}_{vis} + \mathbf{k}_{vis} + \mathbf{k}_{IR} = \mathbf{k}_{IR}$, is under interferometric detection.

To extract information on the nonlinear molecular response against the three pulses, one can measure the phase and amplitude of the third-order signal field, which is possible by employing a heterodyne detection method in the frequency domain. The signal field E_s is allowed to interfere with a local oscillator (LO) pulse E_0 that is another IR pulse delayed from the $\mathbf{k}_{IR} = \mathbf{k}_3$(IR) pulse. The interference signal, which is given by $I_h(\omega_t, T, \tau) = 2\mathrm{Re}\,[E_0^*(\omega_t)E_s(\omega_t, T, \tau)]$, is what is measured in the frequency (ω_t) domain. Note that the Fourier transform of the t-dependent signal electric field, $E_s(t, T, \tau)$, is performed by a grating, and the conjugate frequency was denoted as ω_t. The complex 2DEV signal field can be extracted from $I_h(\omega_t, T, \tau)$, i.e.,[36,37]

$$E_s(\omega_t, T, \tau) = \frac{F[\theta(t)\, F^{-1}\{I_h(\omega_t, T, \tau)\}]\, e^{-i\omega_t\Delta_\tau}}{E_0^*(\omega_t)} \tag{26}$$

where F and F^{-1} mean the Fourier and inverse Fourier transform, respectively, and Δ_τ is the time delay between the $\mathbf{k}_{IR}$ pulse and the LO pulse. The full 2DEV spectrum is finally obtained by performing a numerical Fourier transformation of $E_s(\omega_t, T, \tau)$ with respect to the delay time, τ, between the first and second pulses as

$$\tilde{E}_s(\omega_t, T, \omega_\tau) = \int_{-\infty}^{\infty} d\tau\, E_s(\omega_t, T, \tau)\exp(i\omega_\tau\tau) \tag{27}$$

From the theoretical expression of the third-order polarization in eq 11, we find the polarization that is the radiation source for the emitted signal field in the direction of $\mathbf{k}_{IR}$, as

$$\boldsymbol{P}_s(\mathbf{r}, t, T, \tau) = \{\mathbf{P}_{s1}(t, T, \tau) + \mathbf{P}_{s2}(t, T, \tau)\}\exp(i\boldsymbol{k}_{IR}\cdot\mathbf{r} - i\omega_{IR}t) \tag{28}$$

where the two amplitude terms are

$$\mathbf{P}_{s1}(t, T, \tau) = \left(\frac{i}{\hbar}\right)^3\int_0^\infty dt_1\int_0^\infty dt_2\int_0^\infty dt_3\, \mathbf{R}(t_3, t_2, t_1)\vdots\mathbf{E}_3(t - t_3)\mathbf{E}_2(t + T - t_3 - t_2) \times \mathbf{E}_1^*(t + \tau + T - t_3 - t_2 - t_1)\exp\{i\omega_{IR}t_3 - i\omega_{vis}t_1\}$$

$$\boldsymbol{P}_{s2}(t, T, \tau) = \left(\frac{i}{\hbar}\right)^3\int_0^\infty dt_1\int_0^\infty dt_2\int_0^\infty dt_3\, \boldsymbol{R}(t_3, t_2, t_1)\vdots\mathbf{E}_3(t - t_3)\,\mathbf{E}_2^*(t + T - t_3 - t_2) \mathbf{E}_1(t + \tau + T - t_3 - t_2 - t_1)\exp\{i\omega_{IR}t_3 + i\omega_{vis}t_1\} \tag{29}$$

The center frequencies of the visible and IR pulses in eq 29 are denoted as ω_{vis} and ω_{IR}, and $\mathbf{E}_j(t) = \boldsymbol{\varepsilon}_j e_j(t)$ where $\boldsymbol{\varepsilon}_j$ and $e_j(t)$ are the unit vector representing the polarization direction and the temporal envelop function of the jth pulse. Among many terms in the third-order response function $\mathbf{R}(t_3, t_2, t_1)$, only those involving resonant electronic and vibrational transitions induced by the incident visible and IR fields will significantly contribute to the signal. The first term in eq 28, $\mathbf{P}_{s1}(t, T, \tau)$, in the case of the degenerate pump−probe spectroscopy with the same pump and probe center frequencies is related to the rephasing contribution to the signal, whereas the second term, $\mathbf{P}_{s2}(t, T, \tau)$, is often referred to as a nonrephasing contribution.[2] When this pump−probe geometry is used to carry out 2DEVS measurements, both the rephasing and nonrephasing terms contribute to the measured signal.

Short-Time Approximated Expression for the 2DEV Spectrum. Since both the electronically excited and ground states have manifolds of vibrational states, it is necessary to include all the possible vibronic transitions to describe the 2DEV spectroscopy. For the sake of notational simplicity, let us consider one vibrational mode even though it is a straightforward exercise to generalize the present theory for molecular systems with multiple normal modes. Hereafter, $|g\rangle$ and $|g'\rangle$ denote the vibrationally ground and first excited states in the electronic ground state, respectively, whereas $|e\rangle$, $|e'\rangle$, and $|e''\rangle$ are the vibrationally ground, first excited, second excited states, respectively, in the vibrational manifold of the electrically excited state.

In the present subsection, we shall focus on the rephasing term $\mathbf{P}_{s1}(t, T, \tau)$ only. One can perform the same line of derivation to obtain the formal expression for the nonrephasing term $\mathbf{P}_{s2}(t, T, \tau)$. If the visible field is resonant with the electronic transition between $|g\rangle$ and $|e\rangle$, there are two terms in the $\mathbf{R}(t_3, t_2, t_1)$ that satisfy the phase-matching requirement and both electronic and vibrational resonance conditions. Their double-sided Feynman diagrams contributing to $\mathbf{P}_{s1}(t, T, \tau)$ are shown in Figure 2. The transition pathway A corresponds to the case that the first two field−matter interactions with visible field bleach the electronic ground state molecules. The third interaction of the pump-perturbed system with the third pulse in the IR frequency domain brings

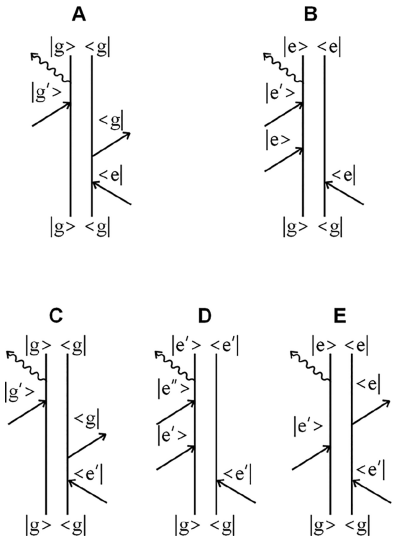

Figure 2. Double-sided Feynman diagrams. Diagrams A and B are associated with the positive and negative 2DEV peaks at ($\omega_t = \bar{\omega}_{g'g}$, $\omega_\tau = \bar{\omega}_{e'g}$) and ($\omega_t = \bar{\omega}_{e'e}$, $\omega_\tau = \bar{\omega}_{e'g}$), respectively, which are referred to as GB and EA contributions to the 2DEV signal. Diagrams C−E describe the Liouville space pathways representing the nonlinear optical transitions resulting in the triplet at ($\omega_\tau = \bar{\omega}_{e'g}$) consisting of the GB, EA, and SE peaks at ($\omega_t = \bar{\omega}_{g'g}$, $\omega_\tau = \bar{\omega}_{e'g}$), ($\omega_t = \bar{\omega}_{e''e}$, $\omega\tau = \bar{\omega}_{e'g}$), and ($\omega_t = \bar{\omega}_{e'e}$, $\omega_\tau = \bar{\omega}_{e'g}$).

https://dx.doi.org/10.1021/acs.jpcb.0c08959
J. Phys. Chem. B 2020, 124, 11222−11235

the system into a vibrational coherence, i.e., a superposition state of $|g\rangle$ and $|g'\rangle$, which oscillates in time t with an angular frequency of $\omega_{g'g}$. The expectation value of the dipolar operator over the third-order density matrix, which corresponds to the molecular polarization induced by the third-order field−matter interactions by definition, oscillates in time. The third-order polarization $\mathbf{P}_{s1}(t, T, \tau)$ acts like a Hertzian dipole emitting an electromagnetic wave whose propagation direction is parallel to the vector of $-\mathbf{k}_{vis} + \mathbf{k}_{vis} + \mathbf{k}_{IR}$ due to the principle of momentum conservation. Comparing the double-sided Feynman diagram associated with the transition pathway A with that of R_2 in Figure 1, we find that the pathway A is similar to the ground-state bleach (GB) term in the conventional 2D electronic or IR spectroscopy.[30] However, because of the mixed (electronic and vibrational) transitions involved in the 2DEV spectroscopy, pathway A represents the case that the vibrational ground state is bleached by the electronic excitation, not by an IR excitation. Hereafter, we shall refer to this term as GB.

Transition pathway B differs from A because the system evolves on the potential energy surface of an electronically excited state during the waiting time T. Then, an absorptive interaction of the IR pulse with the molecular system creates a superposition state of $|e\rangle$ and $|e'\rangle$, which generates the third-order signal electric field along the direction of $-\mathbf{k}_{vis} + \mathbf{k}_{vis} + \mathbf{k}_{IR}$. The net effect from this polarization component associated with pathway B on the IR beam is that a single IR photon is absorbed (annihilated) by the molecule that was electronically excited by the pair of visible pulses. Therefore, this contribution from pathway B can be referred to as the excited-state absorption (EA).

Comparing the double-sided Feynman diagrams associated with the transition pathways A and B in Figure 2 with those in Figure 1, we find that the two terms GB and EA correspond to $R_3(t_3, t_2, t_1)$ and $-R_3^*(t_3, t_2, t_1)$, respectively. Using the short-time approximate expressions for these two components, the third-order polarization components that are associated with the positive 2DEV peak at $(\omega_t = \bar{\omega}_{g''g}, \omega_\tau = \bar{\omega}_{eg})$ and the negative 2DEV peak at $(\omega_t = \bar{\omega}_{e',e}, \omega_\tau = \bar{\omega}_{eg})$ are given as

$$
\begin{aligned}
\mathbf{P}_{s1}(t, T, \tau) = {} & -i\hbar^{-3}\boldsymbol{\mu}_{gg'}(\boldsymbol{\mu}_{g'g}\cdot\boldsymbol{\varepsilon}_3)(\boldsymbol{\mu}_{eg}\cdot\boldsymbol{\varepsilon}_2)(\boldsymbol{\mu}_{ge}\cdot\boldsymbol{\varepsilon}_1^*) \\
& \times \int_0^\infty dt_1 \int_0^\infty dt_2 \int_0^\infty dt_3 \exp\{-\langle\delta\omega_{g'g}^2\rangle_c t_3^2/2 - \langle\delta\omega_{eg}^2\rangle_c \\
& \times t_1^2/2 + \langle\delta\omega_{eg}(t_2)\delta\omega_{g'g}(0)\rangle_c t_3 t_1\} \\
& \times \exp\{i(\omega_{IR} - \bar{\omega}_{g'g})t_3 - i(\omega_{vis} - \bar{\omega}_{eg})t_1\} \\
& \times e_3(t - t_3)\, e_2(t + T - t_3 - t_2) \times \\
& e_1(t + \tau + T - t_3 - t_2 - t_1) + i\hbar^{-3}\boldsymbol{\mu}_{ee'}(\boldsymbol{\mu}_{e'e}\cdot\boldsymbol{\varepsilon}_3)(\boldsymbol{\mu}_{eg}\cdot\boldsymbol{\varepsilon}_2) \\
& \times (\boldsymbol{\mu}_{ge}\cdot\boldsymbol{\varepsilon}_1^*) \int_0^\infty dt_1 \int_0^\infty dt_2 \int_0^\infty dt_3 \exp\{-\langle\delta\omega_{e'e}^2\rangle_c t_3^2/2 \\
& - \langle\delta\omega_{eg}^2\rangle_c t_1^2/2 + \langle\delta\omega_{eg}(t_2)\,\delta\omega_{e'e}(0)\rangle_c t_3 t_1\} \\
& \times \exp\{i(\omega_{IR} - \bar{\omega}_{e'e} + \beta\hbar(\langle\delta\omega_{eg}(t_2)\,\delta\omega_{e'e}(0)\rangle_c \\
& - \langle\delta\omega_{eg}\delta\omega_{e'e}\rangle_c))t_3 - i(\omega_{vis} - \bar{\omega}_{eg})t_1\} e_3(t - t_3) \\
& \times e_2(t + T - t_3 - t_2)\, e_1(t + \tau + T - t_3 - t_2 - t_1)
\end{aligned}
\tag{30}
$$

Here, $\boldsymbol{\mu}_{eg}$ ($\boldsymbol{\mu}_{ge}$) are the electronic transition dipole moments, and $\boldsymbol{\mu}_{g'g}$ ($\boldsymbol{\mu}_{gg'}$) and $\boldsymbol{\mu}_{e'e}$ ($\boldsymbol{\mu}_{ee'}$) are the vibrational transition dipole moments of the same normal mode in the electronic ground and excited states, respectively. From now on, the unit polarization vectors $\boldsymbol{\varepsilon}_j$ are assumed to be real. To obtain the above result in eq 30, we used a classical approximation to the FFCFs. Within this classical approximation, the imaginary part of the FFCF, denoted as $C_I(t)$ is related to the real part of the FFCF $C_R(t)$ as[1,2,30]

$$
C_I(t) \cong -\frac{\beta\hbar}{2}\frac{d}{dt} C_R(t) \tag{31}
$$

where $\beta = 1/k_B T$, k_B is the Boltzmann constant, and T is the temperature. The real part of the quantum correlation function is assumed to be the classical FFCF.[30] In eq 30 and hereafter, $\langle ... \rangle_c$ refers to the classical correlation function. These classical or high-temperature approximations are acceptable because the bath degrees of freedom, which are often modeled as a collection of harmonic oscillators, can be treated as classical quantities in the phase space instead of operators in the Liouville space. More specifically, the fluctuations of both the electronic and vibrational transition frequencies are induced by the solute−solvent dynamics. The coupled bath degrees of freedom are low-frequency modes whose frequencies are usually smaller than approximately 200 cm^{-1} ($= k_B T/hc$, where c is the speed of light in cm/s) at room temperature. However, if the temperature decreases, then the high-temperature approximation breaks down. Because both the FFCFs of electronic and vibrational transition frequencies decay due to the fluctuation of the same set of bath degrees of freedom, such breakdowns of high-temperature approximation would not occur at significantly different temperatures for the vibrational and electronic transition frequency fluctuations.

If the temporal envelops of the visible and IR pulses are sufficiently shorter than the electronic dephasing time and the vibrational dephasing time, respectively, then they can be replaced with the corresponding Dirac delta functions. However, the spectral bandwidths of these pulses are not assumed to be infinitely broad because in practical experiments the finite bandwidths of the visible and IR pulses are just broad enough to cover the vibrational manifold of an electronically excited state. Here, we ignore the vibrational coherence evolutions during T_w, which are generated by Raman interactions of optical chromophores with the visible pump beams. Then, the third-order polarization amplitude in eq 30 after performing triple integrations becomes simplified as

$$
\begin{aligned}
\mathbf{P}_{s1}(t, T, \tau) = {} & -i\hbar^{-3}\boldsymbol{\mu}_{gg'}(\boldsymbol{\mu}_{g'g}\cdot\boldsymbol{\varepsilon}_3)(\boldsymbol{\mu}_{eg}\cdot\boldsymbol{\varepsilon}_2)(\boldsymbol{\mu}_{ge}\cdot\boldsymbol{\varepsilon}_1) \\
& \times \exp\{-\langle\delta\omega_{g'g}^2\rangle_c t^2/2 - \langle\delta\omega_{eg}^2\rangle_c \tau^2/2 + \langle\delta\omega_{eg}(T)\,\delta\omega_{g'g}(0)\rangle_c t\tau\} \\
& \times \exp\{i(\omega_{IR} - \bar{\omega}_{g'g})t - i(\omega_{vis} - \bar{\omega}_{eg})\tau\} + i\hbar^{-3}\boldsymbol{\mu}_{ee'}(\boldsymbol{\mu}_{e'e}\cdot\boldsymbol{\varepsilon}_3) \\
& (\boldsymbol{\mu}_{eg}\cdot\boldsymbol{\varepsilon}_2)(\boldsymbol{\mu}_{ge}\cdot\boldsymbol{\varepsilon}_1)\exp\{-\langle\delta\omega_{e'e}^2\rangle_c t^2/2 - \langle\delta\omega_{eg}^2\rangle_c \tau^2/2 \\
& + \langle\delta\omega_{eg}(T)\,\delta\omega_{e'e}(0)\rangle_c t\tau\}\exp\{i(\omega_{IR} - \bar{\omega}_{e'e} \\
& + \beta\hbar(\langle\delta\omega_{eg}(T)\,\delta\omega_{e'e}(0)\rangle_c - \langle\delta\omega_{eg}\delta\omega_{e'e}\rangle_c))t - i(\omega_{vis} - \bar{\omega}_{eg})\tau\}
\end{aligned}
\tag{32}
$$

Using the slowly varying amplitude approximation when solving the Maxwell equation with a radiation source given by the above polarization, one can find that the signal electric field amplitude $\mathbf{E}_{s1}(t, T, \tau)$ is proportional to $\mathbf{P}_{s1}(t, T, \tau)$ as

https://dx.doi.org/10.1021/acs.jpcb.0c08959
J. Phys. Chem. B 2020, 124, 11222−11235

$\mathbf{E}_{s1}(t, T, \tau) \propto i\,\mathbf{P}_{s1}(t, T, \tau)$. After carrying out the 2D Fourier–Laplace transformation of $\mathbf{E}_{s1}(t, T, \tau)$ with respect to τ and t,

$$\tilde{\mathbf{E}}_{s1}(\tilde{\omega}_t, T, \tilde{\omega}_\tau) = \int_0^\infty dt \int_0^\infty d\tau\, \mathbf{E}_{s1}(t, T, \tau) \exp(i\tilde{\omega}_t t + i\tilde{\omega}_\tau \tau) \tag{33}$$

and introducing two frequencies as $\omega_\tau \equiv \omega_{vis} - \tilde{\omega}_\tau$ and $\omega_t \equiv \omega_{IR} + \tilde{\omega}_t$ we could obtain the waiting time (T)-dependent 2DEV spectrum

$$\tilde{\mathbf{E}}_{s1}(\omega_t, T, \omega_\tau) = \tilde{\mathbf{E}}_{s1}^{GB}(\omega_t, T, \omega_\tau) + \tilde{\mathbf{E}}_{s1}^{EA}(\omega_t, T, \omega_\tau) \tag{34}$$

where

$$\tilde{\mathbf{E}}_{s1}^{GB}(\omega_t, T, \omega_\tau) \propto \frac{\boldsymbol{\mu}_{gg'}(\boldsymbol{\mu}_{g'g}\cdot\boldsymbol{\epsilon}_3)(\boldsymbol{\mu}_{eg}\cdot\boldsymbol{\epsilon}_2)(\boldsymbol{\mu}_{ge}\cdot\boldsymbol{\epsilon}_1)}{\langle\delta\omega_{eg}^2\rangle_c^{1/2}\left(\langle\delta\omega_{g'g}^2\rangle_c - \frac{\langle\delta\omega_{eg}(T)\,\delta\omega_{g'g}(0)\rangle_c^2}{\langle\delta\omega_{eg}^2\rangle_c}\right)^{1/2}} \exp\{-x^2(\omega_\tau)\}\{\exp\{-z^2(\omega_t, T, \omega_\tau)\} + \frac{2i}{\sqrt{\pi}}F\{z(\omega_t, T, \omega_\tau)\}\}$$

$$\tilde{\mathbf{E}}_{s1}^{EA}(\omega_t, T, \omega_\tau) \propto -\frac{\boldsymbol{\mu}_{ee'}(\boldsymbol{\mu}_{e'e}\cdot\boldsymbol{\epsilon}_3)(\boldsymbol{\mu}_{eg}\cdot\boldsymbol{\epsilon}_2)(\boldsymbol{\mu}_{ge}\cdot\boldsymbol{\epsilon}_1)}{\langle\delta\omega_{eg}^2\rangle_c^{1/2}\left(\langle\delta\omega_{e'e}^2\rangle_c - \frac{\langle\delta\omega_{eg}(T)\,\delta\omega_{e'e}(0)\rangle_c^2}{\langle\delta\omega_{eg}^2\rangle_c}\right)^{1/2}} \exp\{-x^2(\omega_\tau)\}\{\exp\{-w^2(\omega_t, T, \omega_\tau)\} + \frac{2i}{\sqrt{\pi}}F\{w(\omega_t, T, \omega_\tau)\}\} \tag{35}$$

$F(x)$ is the Dawson integral. The auxiliary functions in eq 34 are defined as

$$x(\omega_\tau) \equiv \frac{\omega_\tau - \bar{\omega}_{eg}}{\sqrt{2\langle\delta\omega_{eg}^2\rangle_c}}$$

$$z(\omega_t, T, \omega_\tau) \equiv \frac{\omega_t - \bar{\omega}_{g'g} - \frac{\langle\delta\omega_{eg}(T)\delta\omega_{g'g}(0)\rangle_c}{\langle\delta\omega_{eg}^2\rangle_c}(\omega_\tau - \bar{\omega}_{eg})}{\sqrt{2\left(\langle\delta\omega_{g'g}^2\rangle_c - \frac{\langle\delta\omega_{eg}(T)\delta\omega_{g'g}(0)\rangle_c^2}{\langle\delta\omega_{eg}^2\rangle_c}\right)}}$$

$$w(\omega_t, T, \omega_\tau) \equiv \frac{\omega_t - \bar{\omega}_{e'e} + \beta\hbar(\langle\delta\omega_{eg}(T)\delta\omega_{e'e}(0)\rangle_c - \langle\delta\omega_{eg}\delta\omega_{e'e}\rangle_c) - \frac{\langle\delta\omega_{eg}(T)\,\delta\omega_{e'e}(0)\rangle_c}{\langle\delta\omega_{eg}^2\rangle_c}(\omega_\tau - \bar{\omega}_{eg})}{\sqrt{2\left(\langle\delta\omega_{e'e}^2\rangle_c - \frac{\langle\delta\omega_{eg}(T)\,\delta\omega_{e'e}(0)\rangle_c^2}{\langle\delta\omega_{eg}^2\rangle_c}\right)}} \tag{36}$$

Similarly, one can obtain the expressions for $\tilde{\mathbf{E}}_{s2}^{GB}(\omega_t, T, \omega_\tau)$, $\tilde{\mathbf{E}}_{s2}^{EA}(\omega_t, T, \omega_\tau)$, and $\tilde{\mathbf{E}}_{s2}(\omega_t, T, \omega_\tau)$, which are associated with the nonrephasing diagrams contributing to the pump–probe-type 2DEV signal. Combining these results, we find that the measured 2DEV spectrum, which is the sum of rephasing and nonrephasing terms, is given by the real parts of $\tilde{\mathbf{E}}_{s1}^{GB}(\omega_t, T, \omega_\tau)$, $\tilde{\mathbf{E}}_{s1}^{EA}(\omega_t, T, \omega_\tau)$, and $\tilde{\mathbf{E}}_{s1}(\omega_t, T, \omega_\tau)$. That is to say, the 2DEV spectrum is given as

$$\begin{aligned}\tilde{\mathbf{E}}_s(\omega_t, T, \omega_\tau) &= \tilde{\mathbf{E}}_{s1}(\omega_t, T, \omega_\tau) + \tilde{\mathbf{E}}_{s2}(\omega_t, T, \omega_\tau) \\ &= 2Re\{\tilde{\mathbf{E}}_{s1}^{GB}(\omega_t, T, \omega_\tau) + \tilde{\mathbf{E}}_{s1}^{EA}(\omega_t, T, \omega_\tau)\}\end{aligned} \tag{37}$$

This is one of the principal results in this paper. From eqs 34–37, it turns out that the 2DEV line shape is a rotated 2D Gaussian function for ω_τ and ω_t. Both the angle of rotation and the degree of elongation depend on the waiting time, which is the subject that will be discussed in detail later in this article. Here, it should be mentioned that due to the breakdowns of the short-time approximation to the third-order response function and the impulsive pulse approximation the result for the 2DEV spectrum is not valid at very short waiting times. Furthermore, when the incident pulses overlap in time, the time-ordering of the field–matter interactions is not well-defined, so a few more pathways will contribute to the measured signal. Usually, the 2DEVS spectrum is plotted with respect to the two Fourier frequencies for quantitatively interpreting the time-resolved spectra, which is known as the frequency-versus-frequency plotting convention. However, Cina's group shows that the time-versus-time interpretation of the 2D electronic signals is useful and advantageous over the frequency-versus-frequency analysis when pulse overlaps make the interpretation of the experimental results complicated.[38] Hereafter, we shall follow the frequency-versus-frequency plotting convention and focus on the case when the above two approximations are acceptable and when the pulses do not strongly overlap in time.

Selection Rule of the 2DEV Spectroscopy. It is well-known that the potential anharmonicity of a given normal mode is needed to make the 2DIR spectroscopic signal nonzero. For 2DES, the signal becomes nonzero because of the non-Bosonic character of the electronic transition, e.g., a two-level system. Interestingly, 2DEVS has a different set of selection rules. The GB and EA positively and negatively contribute to the signal, respectively, but they can largely cancel out with each other when the vibrational transition frequency $\bar{\omega}_{g'g}$ of a given normal mode in the electronic ground state is identical or close to $\bar{\omega}_{e'e}$ in the electronically excited state. However, even in the case that $\bar{\omega}_{g'g} = \bar{\omega}_{e'e}$, if the vibronic coupling constant, i.e., Huang–Rhys factor, for this normal mode is nonzero, if the vibrational transition dipoles differ from each other, i.e., $\boldsymbol{\mu}_{g'g} \neq \boldsymbol{\mu}_{e'e}$, if the solvation-induced Stokes shift of the electronic transition frequency is not negligibly small, i.e., $\langle\delta\omega_{eg}\delta\omega_{e'e}\rangle_c \neq 0$, or if the electronic-vibrational FFCFs, e.g., $\langle\delta\omega_{eg}(T)\,\delta\omega_{g'g}(0)\rangle_c$ and $\langle\delta\omega_{eg}(T)\,\delta\omega_{e'e}(0)\rangle_c$, substantially differ from each other, then the cancellation between the GB and EA terms is not perfect. Therefore, the observation of nonzero

https://dx.doi.org/10.1021/acs.jpcb.0c08959
J. Phys. Chem. B 2020, 124, 11222–11235

2DEV signal results from one or some combination of the above cases. Furthermore, if molecules are electronically coupled, creating vibronic excitons, then a second factor enters the 2DEV spectrum. The transition moments of infrared transitions in the excited state manifold can be very significantly altered from their monomer values, and vibronic transitions that are weak in the linear electronic absorption spectrum can appear prominently in the 2DEV spectrum.[39]

Time-Dependent 2DEV Spectrum. From eq 35, the GB contribution to the real part of the signal is a 2D Gaussian function with a positive peak at $\omega_\tau = \bar{\omega}_{eg}$ and $\omega_t = \bar{\omega}_{g'g}$. The EA contribution to $\tilde{\mathbf{E}}_s(\omega_t, T, \omega_\tau)$, which is also a 2D Gaussian function, peaks at $\omega_\tau = \bar{\omega}_{eg}$ and $\omega_t = \bar{\omega}_{e'e} - \beta\hbar(\langle\delta\omega_{eg}(T)\,\delta\omega_{e'e}(0)\rangle_c - \langle\delta\omega_{eg}\,\delta\omega_{e'e}(0)\rangle_c$ (Figure 3, features A and B). Due

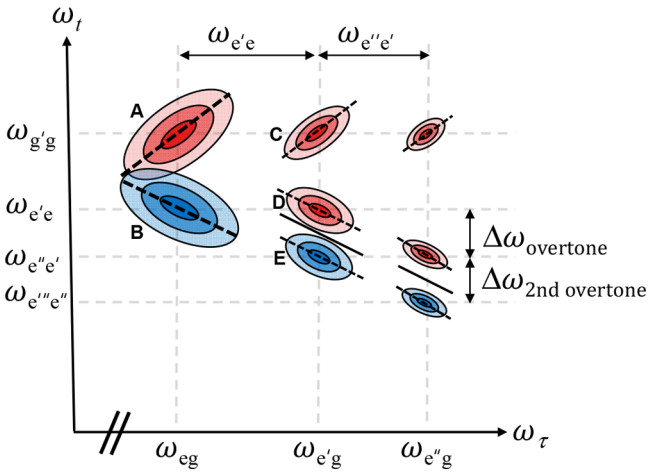

Figure 3. Schematic diagram of the 2DEV spectrum. The positive and negative peaks are shown in red and blue, respectively. The dashed and solid lines are the center and nodal lines, respectively.

to the cross FFCF, $\langle\delta\omega_{eg}(T)\,\delta\omega_{e'e}(0)\rangle_c$, which is the spectral diffusion process, the center frequency of the negative EA peak shifts along the ω_t axis as the waiting time increases, which is the spectral diffusion process or solvation dynamics[31] contributing to the negative EA peak in the 2DEV spectrum.

The 2D GB and EA peaks in the 2DEV spectrum, $\tilde{\mathbf{E}}_s(\omega_t, T, \omega_\tau)$, at short waiting times could be diagonally or anti-diagonally elongated due to the quasi-instantaneous heterogeneity of local environments around chromophores, which gives rise to the distribution of electronic and vibrational transition frequencies. What is interesting and different from the conventional 2DES or 2DIR spectroscopy is that the time-correlation between the fluctuating electronic transition frequency and the fluctuating vibrational transition frequency can be measured through the analysis of the 2DEV spectra. The slope of 2DEV peak indicates the following inequalities, for the GB and EA peaks, respectively:

$$\langle\delta\omega_{eg}\delta\omega_{g'g}\rangle_c \neq 0$$
$$\langle\delta\omega_{eg}\delta\omega_{e'e}\rangle_c \neq 0 \tag{38}$$

As the waiting time T increases, each 2D peak becomes symmetric with respect to ω_τ and ω_t. Such a waiting-time-dependent change in the diagonally or anti-diagonally elongated peak shape can be quantitatively characterized by measuring the CLS of each 2DEV peak. From the approximate 2D Gaussian functions for the GB and EA peaks, the center line slopes are given by

$$\mathrm{CLS}_{GB}(T) = \frac{\langle\delta\omega_{eg}(T)\,\delta\omega_{g'g}(0)\rangle_c}{\langle\delta\omega_{eg}^2\rangle_c}$$
$$\mathrm{CLS}_{EA}(T) = \frac{\langle\delta\omega_{eg}(T)\,\delta\omega_{e'e}(0)\rangle_c}{\langle\delta\omega_{eg}^2\rangle_c} \tag{39}$$

The results above suggest that the chromophore−solvent-interaction-induced spectral diffusion processes of both the electronic and vibrational transitions are correlated with each other via the couplings of the electronic and vibrational degrees of freedom with the same solvent (bath) modes. If the two fluctuations are coupled to completely independent solvent modes, then the CLS value should be zero even in the case that the inhomogeneous distributions of the electronic and vibrational transition frequencies are large. We will get back to this point later in this paper.

From eq 39, the short-time CLS is determined by the ratio of the cross-correlation amplitude to the mean square fluctuation of the electronic transition frequency, i.e., $\langle\delta\omega_{eg}\delta\omega_{g'g}\rangle_c/\langle\delta\omega_{eg}^2\rangle_c$ and $\langle\delta\omega_{eg}\delta\omega_{e'e}\rangle_c/\langle\delta\omega_{eg}^2\rangle_c$, which are usually less than unity in magnitude because the electronic dephasing time constants are larger than the vibrational dephasing time constants:

$$-1 \le \frac{\langle\delta\omega_{eg}\delta\omega_{g'g}\rangle_c}{\langle\delta\omega_{eg}^2\rangle_c} \le 1$$
$$-1 \le \frac{\langle\delta\omega_{eg}\delta\omega_{e'e}\rangle_c}{\langle\delta\omega_{eg}^2\rangle_c} \le 1 \tag{40}$$

The ranges of cross-correlation amplitudes indicate that the instantaneous heterogeneity of the local environments around chromophores, which results in the distribution of electronic transition frequencies, makes the CLS of a given 2DES peak nonzero only when the two sets of bath degrees of freedom that are responsible for the electronic and vibrational dephasing processes are coherently coupled to these two distinctively different molecular transition processes. Furthermore, the slope of the center line or nodal line in the 2DEV spectrum is not necessarily positive. The magnitude and sign of the normalized cross-correlation functions are determined by the correlation between the solvation-induced shifts of the electronic and vibrational transition frequencies.

If the vibrational transition frequency $\bar{\omega}_{g'g}$ of a given mode in the electronic ground state is different from that $\bar{\omega}_{e'e}$ of the same mode in the electronically excited state, then the positive GB peak and the negative EA peak are aligned vertically at $\omega_\tau = \bar{\omega}_{eg}$ (peaks A and B in Figure 3). We note that the x-axis of the 2D frequency map is ω_τ. Then, the nodal line separating the positive and negative peaks has a finite slope at short waiting times, and its slope is approximately determined by the average FFCFs which is $\{\langle\delta\omega_{eg}(T)\,\delta\omega_{g'g}(0)\rangle_c + \langle\delta\omega_{eg}(T)\,\delta\omega_{e'e}(0)\rangle_c\}/\langle\delta\omega_{eg}^2\rangle_c$.

Although the theoretical description of 2DEVS given above did not take into consideration the static inhomogeneous broadening, following the same line of derivation in ref 2, one can easily include the contributions from the static distributions of both electronic and vibrational transition frequencies. If the variances of the vibrational and electronic

https://dx.doi.org/10.1021/acs.jpcb.0c08959
J. Phys. Chem. B 2020, 124, 11222−11235

transition frequency distributions are σ^2 and Σ^2, then the results in eqs 35 and 36 are to be modified by performing the following replacements:

$$\langle \delta\omega_{g'g}^2 \rangle \rightarrow \langle \delta\omega_{g'g}^2 \rangle + \sigma^2$$
$$\langle \delta\omega_{e'e}^2 \rangle \rightarrow \langle \delta\omega_{e'e}^2 \rangle + \sigma^2$$
$$\langle \delta\omega_{eg}^2 \rangle \rightarrow \langle \delta\omega_{eg}^2 \rangle + \Sigma^2 \tag{41}$$

In addition, if the static inhomogeneities of the electronic and vibrational transition frequencies affect the cross-correlation function, then the corresponding FFCFs in eq 39 could have the corresponding offset values.

Vibrational Progression in the Electronically Excited State. In the above, we considered two 2DEV peaks at $\omega_\tau = \bar{\omega}_{eg}$. However, due to the presence of multiple vibronically coupled states in the electronically excited state, the vibronic transitions from $|g\rangle$ to $|e'\rangle$, from $|g\rangle$ to $|e''\rangle$, and so on are allowed, where the corresponding electronic transition dipole moment is linearly proportional to the Franck−Condon overlap. Such a series of vibronic transitions is manifested in the linear absorption spectrum that exhibits multiple peaks due to the vibrational progression of a strongly vibronically coupled mode.

Now, let us consider the 2DEV peaks at $\omega_\tau = \bar{\omega}_{e'g}$ which involves an electronic transition from $|g\rangle$ to $|e'\rangle$. Three different pathways C−E are to be included to describe each triplet at $\omega_\tau = \bar{\omega}_{e'g}$. Pathways C and D are similar to pathways A and B, respectively, except that the initial electronic excitation involves the transition between $|g\rangle$ and $|e'\rangle$ instead of that between $|g\rangle$ and $|e\rangle$. They can be referred to as GB and EA terms at $\omega_\tau = \bar{\omega}_{e'g}$. Pathway E involves an electronic transition to $|e'\rangle$, and the system evolves on a population state $|e'\rangle\langle e'|$ during T. Then, the interaction with the IR pulse stimulates an emissive transition from $|e'\rangle$ to $|e\rangle$, which is similar to the stimulated emission (SE) contribution to the 2DIR signal except that the creation of the population on a vibrationally excited state is induced by the electronic transitions instead. Therefore, we shall refer to the pathway E as the SE term.

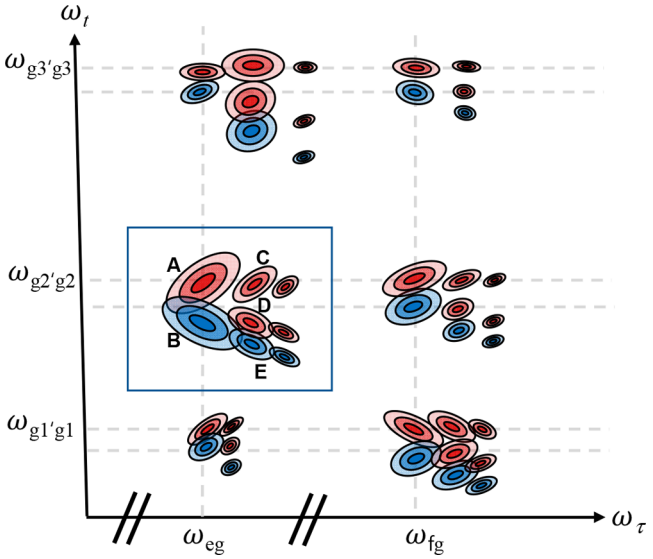

Figure 4. Schematic diagram of the broadband 2DEV spectrum. If the visible pulse were broad enough to cover more than one electronic transition, then the measured 2DEV spectrum would exhibit multiple groups of peaks with different intensities, frequencies, line shapes, and center line slopes that depend on the associated electronic transition and vibrational mode. The peaks in the blue box in this figure are those in Figure 3.

Following the same line of derivation, we could obtain the waiting time (T)-dependent triplet of 2DEV peaks at $\omega_\tau = \bar{\omega}_{e'g}$ as

$$\tilde{\mathbf{E}}_s(\omega_t, T, \omega_\tau) = \tilde{\mathbf{E}}_s^{GB}(\omega_t, T, \omega_\tau) + \tilde{\mathbf{E}}_s^{EA}(\omega_t, T, \omega_\tau) + \tilde{\mathbf{E}}_s^{SE}(\omega_t, T, \omega_\tau) \tag{42}$$

where

$$\tilde{\mathbf{E}}_s^{GB}(\omega_t, T, \omega_\tau) \propto \frac{\boldsymbol{\mu}_{gg'}(\boldsymbol{\mu}_{g'g}\cdot\boldsymbol{\varepsilon}_3)(\boldsymbol{\mu}_{e'g}\cdot\boldsymbol{\varepsilon}_2)(\boldsymbol{\mu}_{ge'}\cdot\boldsymbol{\varepsilon}_1)}{\langle \delta\omega_{e'g}^2 \rangle_c^{1/2}\left(\langle \delta\omega_{g'g}^2 \rangle_c - \frac{\langle \delta\omega_{e'g}(T)\delta\omega_{g'g}(0)\rangle_c^2}{\langle \delta\omega_{e'g}^2 \rangle_c}\right)^{1/2}} \times \exp\{-x^2(\omega_\tau) - z^2(\omega_t, T, \omega_\tau)\}$$

$$\tilde{\mathbf{E}}_s^{EA}(\omega_t, T, \omega_\tau) \propto -\frac{\boldsymbol{\mu}_{e'e''}(\boldsymbol{\mu}_{e''e'}\cdot\boldsymbol{\varepsilon}_3)(\boldsymbol{\mu}_{e'g}\cdot\boldsymbol{\varepsilon}_2)(\boldsymbol{\mu}_{ge'}\cdot\boldsymbol{\varepsilon}_1)}{\langle \delta\omega_{e'g}^2 \rangle_c^{1/2}\left(\langle \delta\omega_{e''e'}^2 \rangle_c - \frac{\langle \delta\omega_{e'g}(T)\delta\omega_{e''e'}(0)\rangle_c^2}{\langle \delta\omega_{e'g}^2 \rangle_c}\right)^{1/2}} \times \exp\{-x^2(\omega_\tau) - w^2(\omega_t, T, \omega_\tau)\}$$

$$\tilde{\mathbf{E}}_s^{SE}(\omega_t, T, \omega_\tau) \propto \frac{\boldsymbol{\mu}_{ee'}(\boldsymbol{\mu}_{e'e}\cdot\boldsymbol{\varepsilon}_3)(\boldsymbol{\mu}_{e'g}\cdot\boldsymbol{\varepsilon}_2)(\boldsymbol{\mu}_{ge'}\cdot\boldsymbol{\varepsilon}_1)}{\langle \delta\omega_{e'g}^2 \rangle_c^{1/2}\left(\langle \delta\omega_{e'e}^2 \rangle_c - \frac{\langle \delta\omega_{e'g}(T)\delta\omega_{e'e}(0)\rangle_c^2}{\langle \delta\omega_{e'g}^2 \rangle_c}\right)^{1/2}} \times \exp\{-x^2(\omega_\tau) - y^2(\omega_t, T, \omega_\tau)\} \tag{43}$$

The auxiliary functions in eqs 43 are defined as

https://dx.doi.org/10.1021/acs.jpcb.0c08959
J. Phys. Chem. B 2020, 124, 11222−11235

$$x(\omega_\tau) \equiv \frac{\omega_\tau - \bar{\omega}_{e'g}}{\sqrt{2\langle \delta\omega_{e'g}^2\rangle_c}} \quad z(\omega_t, T, \omega_\tau) \equiv \frac{\omega_t - \bar{\omega}_{g'g} - \frac{\langle \delta\omega_{e'g}(T)\,\delta\omega_{g'g}(0)\rangle_c}{\langle \delta\omega_{e'g}^2\rangle_c}(\omega_\tau - \bar{\omega}_{e'g})}{\sqrt{2\left(\langle \delta\omega_{g'g}^2\rangle_c - \frac{\langle \delta\omega_{e'g}(T)\,\delta\omega_{g'g}(0)\rangle_c^2}{\langle \delta\omega_{e'g}^2\rangle_c}\right)}}$$

$$w(\omega_t, T, \omega_\tau) \equiv \frac{\omega_t - \bar{\omega}_{e''e'} + \beta\hbar(\langle \delta\omega_{e'g}(T)\,\delta\omega_{e''e'}(0)\rangle_c - \langle \delta\omega_{e'g}\delta\omega_{e''e'}\rangle_c) - \frac{\langle \delta\omega_{e'g}(T)\,\delta\omega_{e''e'}(0)\rangle_c}{\langle \delta\omega_{e'g}^2\rangle_c}(\omega_\tau - \bar{\omega}_{e'g})}{\sqrt{2\left(\langle \delta\omega_{e''e'}^2\rangle_c - \frac{\langle \delta\omega_{e'g}(T)\,\delta\omega_{e''e'}(0)\rangle_c^2}{\langle \delta\omega_{e'g}^2\rangle_c}\right)}}$$

$$y(\omega_t, T, \omega_\tau) \equiv \frac{\omega_t - \bar{\omega}_{e'e} - \beta\hbar(\langle \delta\omega_{e'g}(T)\,\delta\omega_{e'e}(0)\rangle_c - \langle \delta\omega_{e'g}\delta\omega_{e'e}\rangle_c) - \frac{\langle \delta\omega_{e'g}(T)\,\delta\omega_{e'e}(0)\rangle_c}{\langle \delta\omega_{e'g}^2\rangle_c}(\omega_\tau - \bar{\omega}_{e'g})}{\sqrt{2\left(\langle \delta\omega_{e'e}^2\rangle_c - \frac{\langle \delta\omega_{e'g}(T)\,\delta\omega_{e'e}(0)\rangle_c^2}{\langle \delta\omega_{e'g}^2\rangle_c}\right)}} \tag{44}$$

The additional SE term has the same sign with the GB term, which can potentially cancel out with the negatively contributing EA peak. Note that the peak position of the EA term is at $\omega_t = \bar{\omega}_{e''e'}$, whereas that of the SE term is at $\omega_t = \bar{\omega}_{e'e}$. Due to the anharmonicity of the normal mode in the electronically excited state, the vibrational transition frequency between $|e\rangle$ and $|e'\rangle$ differs from that between $|e'\rangle$ and $|e''\rangle$ by the amount of $\Delta\omega_{\text{overtone}} = \bar{\omega}_{e''e'} - \bar{\omega}_{e'e}$. Usually, we have $\bar{\omega}_{e'e} > \bar{\omega}_{e''e'}$. Consequently, the SE and EA peaks are separated from each other along the ω_t axis by the amount of anharmonic frequency shift (Figure 3). The appearance of the triplet at $(\omega_\tau = \bar{\omega}_{g'g}, \omega_t = \bar{\omega}_{g'g})$, $(\omega_\tau = \bar{\omega}_{e'g}, \omega_t = \bar{\omega}_{e'e})$, and $(\omega_\tau = \bar{\omega}_{e'g}, \omega_t = \bar{\omega}_{e''e'})$ is an indication of vibrational progression present in the 2DEV spectrum.

The T-dependent center line slopes of the three peaks are different from those of the two peaks at $(\omega_\tau = \bar{\omega}_{eg})$ in general because the initial electronic coherence generated by the first field−matter interaction has a different oscillating frequency. From eqs 43 and 44, the corresponding CLS functions are

$$\text{CLS}_{\text{GB}}(T) = \frac{\langle \delta\omega_{e'g}(T)\,\delta\omega_{g'g}(0)\rangle_c}{\langle \delta\omega_{e'g}^2\rangle_c}$$

$$\text{CLS}_{\text{EA}}(T) = \frac{\langle \delta\omega_{e'g}(T)\,\delta\omega_{e''e'}(0)\rangle_c}{\langle \delta\omega_{e'g}^2\rangle_c}$$

$$\text{CLS}_{\text{SE}}(T) = \frac{\langle \delta\omega_{e'g}(T)\,\delta\omega_{e'e}(0)\rangle_c}{\langle \delta\omega_{e'g}^2\rangle_c} \tag{45}$$

Comparing the CLS changes of the peaks at $(\omega_\tau = \bar{\omega}_{e'g})$ with those at $(\omega_\tau = \bar{\omega}_{e'g})$, one can further extract information on the strength and distribution of the solvent modes that are coupled to the vibrational transition of a given normal mode in the electronically excited state.

In the above discussion, we considered just a single vibrational mode (Q_j) and one electronic transition $(|e\rangle)$. Using broadband IR and visible pulses, one could excite multiple vibrational modes and explore vibronic couplings on the high-lying electronic states. In Figure 4, a schematic representation of the broadband 2DEV spectrum is depicted. The three vibrational modes are differently denoted as $g1$, $g2$, and $g3$, and the second electronically excited state is denoted as $|f\rangle$. The lineshapes of 2DEV spectra would depend on a variety of molecular properties.

Chromophore−Solvent Dynamics and Cross FFCF. To elucidate the nature of cross-correlation of fluctuating vibrational and electronic transition frequencies that are induced by the chromophore−solvent dynamics, we need to consider the theory of solvation dynamics and its interplay with electronic and vibrational frequency fluctuations.

Often, chromophores undergoing an electronic transition are modeled as a simple two-electronic-level system. Due to the difference in the electronic structures (charge distributions) of the electronically excited and ground states, their interaction energies with surrounding solvent molecules differ from each other. Often, the intermolecular interaction potential can be written as a sum of distinctively different terms. For example, the interaction potentials of the electronic ground and excited states denoted as V_g and V_e, respectively, can be approximately written as

$$V_{g/e} = V_{g/e}^{\text{Coul}} + V_{g/e}^{\text{Rep}} + V_{g/e}^{\text{Ind}} + V_{g/e}^{\text{Disp}} + V_{g/e}^{\text{CT}} \tag{46}$$

where the terms on the right-hand side of this equation are the Coulomb interaction, exchange-repulsion, induction, dispersion, and charge-transfer contributions. Depending on the level of theory for the calculation of each term, there exist empirical, semiempirical, and *ab initio* force fields with parameters derived from fitting to the benchmark data or from first principles. The intermolecular interaction potential is usually a complicated function of the atomic coordinates and electronic state of a given chromophoric molecule. Due to the difference in the chromophore−solvent interaction energies of the electronically excited and ground states, one can write the fluctuating part of the electronic transition frequency as

$$\delta\omega_{eg}(\mathbf{q}) = \frac{\delta V_{eg}(\mathbf{q})}{\hbar} = \frac{1}{\hbar}(V_{eg}(\mathbf{q}) - \langle V_{eg}(\mathbf{q})\rangle) \tag{47}$$

where the difference in interaction energy is defined as $V_{eg}(\mathbf{q}) = V_e(\mathbf{q}) - V_g(\mathbf{q})$.

Over the past two decades, the vibrational frequency shift, which is widely referred to as vibrational solvatochromism, induced by the vibrational chromophore−solvent interaction has been extensively studied to describe such vibrational solvatochromic effects on molecular spectra quantitatively.[15,16] Within the weak-coupling approximation, it was shown that the fluctuating parts of the vibrational energy gaps of a normal mode on the electronic excited and ground states, which are

https://dx.doi.org/10.1021/acs.jpcb.0c08959
J. Phys. Chem. B 2020, 124, 11222−11235

$\delta\omega_{g'g}(\mathbf{q})$ and $\delta\omega_{e'e}(\mathbf{q})$, respectively, can be directly related to the intermolecular interaction potential V as[40−42]

$$\begin{aligned}\delta\omega_{g'g}(\mathbf{q}) &= \omega_{g'g}(\mathbf{q}) - \langle\omega_{g'g}(\mathbf{q})\rangle = \frac{1}{\hbar}\delta\hat{F}_g V_g(\mathbf{q}) \\ &= \frac{1}{\hbar}(\hat{F}_g V_g(\mathbf{q}) - \langle\hat{F}_g V_g(\mathbf{q})\rangle) \\ \delta\omega_{e'e}(\mathbf{q}) &= \omega_{e'e}(\mathbf{q}) - \langle\omega_{e'e}(\mathbf{q})\rangle = \frac{1}{\hbar}\delta\hat{F}_e V_e(\mathbf{q}) \\ &= \frac{1}{\hbar}(\hat{F}_e V_e(\mathbf{q}) - \langle\hat{F}_e V_e(\mathbf{q})\rangle)\end{aligned} \tag{48}$$

where the differential operators connecting the chromophore−solvent interaction energies $V_{e/g}$ to the frequency shifts, i.e., vibrational solvatochromic shift, $\delta\omega_{g'g/e'e}(\mathbf{q})$ are defined as[42]

$$\hat{F}_{e/g} = \frac{1}{2M_j\omega_j}\frac{\partial}{\partial Q_j^2}\bigg|_{\mathbf{Q}_{e/g}} - \frac{1}{2M_j\omega_j}\sum_i \frac{g_{ijj}}{M_i\omega_i^2}\frac{\partial}{\partial Q_i}\bigg|_{\mathbf{Q}_{e/g}} \tag{49}$$

In the notation in eq 49, we assume that the normal mode of interest is the jth one among the $3N - 6$ $(3N - 5)$ normal modes of nonlinear (linear) molecules. The reduced mass, vibrational angular frequency, and vibrational coordinate of the jth normal mode are denoted as M_j, ω_j, and Q_j, respectively. The cubic anharmonic coefficient is denoted as g_{ijj}. The first and second derivatives of the intermolecular interaction potential should be calculated at the equilibrium geometry ($\mathbf{Q}_e$ or $\mathbf{Q}_g$) of the chromophore on its electronically excited or ground state for the calculations of the $\delta\omega_{g'g}(\mathbf{q})$ and $\delta\omega_{e'e}(\mathbf{q})$, respectively.

From eq 48, the electronic-vibrational FFCFs in eq 39 can be written as

$$\begin{aligned}\langle\delta\omega_{eg}(T)\,\delta\omega_{g'g}(0)\rangle_c &= \frac{1}{\hbar^2}\langle\delta V_{eg}(\mathbf{q}(T))\,\delta\hat{F}_g V_g(\mathbf{q})\rangle_c \\ \langle\delta\omega_{eg}(T)\,\delta\omega_{e'e}(0)\rangle_c &= \frac{1}{\hbar^2}\langle\delta V_{eg}(\mathbf{q}(T))\,\delta\hat{F}_e V_e(\mathbf{q})\rangle_c\end{aligned} \tag{50}$$

The result in eq 50 shows how the cross-correlation functions are related to and determined by the chromophore−solvent interaction energy.

To understand the theory in eq 50, let us consider a simple model for the electronic and vibrational solvatochromism. If the assumption that the chromophore−solvent interaction is governed by the interaction between solute dipole and solvent electric field, i.e., the Stark effect, is acceptable and valid, then the fluctuating part of the electronic energy gap is

$$\delta V_{eg}(\mathbf{q}) = -(\boldsymbol{\mu}_e - \boldsymbol{\mu}_g)\cdot\mathbf{E}_{\text{solvent}}(\mathbf{q}) = -\Delta\boldsymbol{\mu}_{eg}\cdot\mathbf{E}_{\text{solvent}}(\mathbf{q}) \tag{51}$$

where the electric dipole moments of the electronically excited and ground states are denoted as $\boldsymbol{\mu}_e$ and $\boldsymbol{\mu}_g$. Similarly, let us assume the vibrational Stark effect[43,44] is an acceptable description for the vibrational frequency shift of a given normal mode due to the chromophore−solvent interaction. Then, we have

$$\begin{aligned}\delta\hat{F}_g V_g(\mathbf{q}) &= -(\hat{F}_g\boldsymbol{\mu}_g)\cdot\mathbf{E}_{\text{solvent}}(\mathbf{q}) = -\delta\boldsymbol{\mu}_g\cdot\mathbf{E}_{\text{solvent}}(\mathbf{q}) \\ \delta\hat{F}_e V_e(\mathbf{q}) &= -(\hat{F}_e\boldsymbol{\mu}_e)\cdot\mathbf{E}_{\text{solvent}}(\mathbf{q}) = -\delta\boldsymbol{\mu}_e\cdot\mathbf{E}_{\text{solvent}}(\mathbf{q})\end{aligned} \tag{52}$$

where $\delta\boldsymbol{\mu}_g$ and $\delta\boldsymbol{\mu}_e$ are the vibrational Stark tuning rates of the jth normal mode of the chromophore in its electronically excited and ground state, respectively. Although the vibrational Stark tuning rate $\delta\boldsymbol{\mu}_g$ of a normal mode in the electronic ground state can be measured by using vibrational Stark effect spectroscopy,[44] the measurement of $\delta\boldsymbol{\mu}_e$ has not been performed experimentally even though quantum chemistry calculations of such Stark tuning rates are possible. In the dipole−electric-field interaction model, both the electronic and vibrational transition frequencies or their energy gaps are modulated by the same local electric field created by surrounding solvent molecules. However, it should be emphasized that the corresponding susceptibility constants, i.e., the electronic and vibrational Stark tuning rates, could be different for different electronic transitions and vibrational modes. Using this Stark effect approximation, we could find that the cross FFCFs in eq 39 can be simplified as

$$\begin{aligned}&\langle\delta\omega_{eg}(T)\,\delta\omega_{g'g}(0)\rangle_c = \\ &\quad\frac{1}{\hbar^2}\langle\mathbf{E}_{\text{solvent}}(\mathbf{q}(T))\cdot\{\Delta\boldsymbol{\mu}_{eg}(T)\,\delta\boldsymbol{\mu}_g(0)\}\cdot\mathbf{E}_{\text{solvent}}(\mathbf{q}(0))\rangle_c \\ &\langle\delta\omega_{eg}(T)\,\delta\omega_{e'e}(0)\rangle_c = \\ &\quad\frac{1}{\hbar^2}\langle\mathbf{E}_{\text{solvent}}(\mathbf{q}(T))\cdot\{\Delta\boldsymbol{\mu}_{eg}(T)\,\delta\boldsymbol{\mu}_e(0)\}\cdot\mathbf{E}_{\text{solvent}}(\mathbf{q}(0))\rangle_c\end{aligned} \tag{53}$$

The quantities, $\Delta\boldsymbol{\mu}_{eg}\delta\boldsymbol{\mu}_g$ and $\Delta\boldsymbol{\mu}_{eg}\delta\boldsymbol{\mu}_e$, are the dyadic products of the corresponding two vectorial Stark tuning rates. The decaying patterns of these cross-correlation functions are mainly determined by the relaxation of the time-correlation of the solvent electric field. Often, the solvation dynamics of an electronically excited molecule, which is manifest by the time-dependent fluorescence Stokes shift or photon-echo peak shift, was described by considering the solvent electric field interacting with solute dipole moments.[31]

It should be noted that the magnitude and sign of each cross-correlation function in eq 53 is also determined by the dyadic product, which could depend on the waiting time T. The relative angles between the two vectors $\Delta\boldsymbol{\mu}_{eg}$ and $\delta\boldsymbol{\mu}_g$ for $\langle\delta\omega_{eg}(T)\,\delta\omega_{g'g}(0)\rangle_c$ and between $\Delta\boldsymbol{\mu}_{eg}$ and $\delta\boldsymbol{\mu}_e$ for $\langle\delta\omega_{eg}(T)\,\delta\omega_{e'e}(0)\rangle_c$ in the molecular coordinate system depend on different vibrational modes. Thus, the electronic and vibrational frequency fluctuations could be positively or negatively correlated with each other depending on the components in the dyadic product.

In addition, if the chromophores rotate, undergo conformational changes, or a change in molecular structure via photoexcitation-induced chemical reaction occurs during T, then the corresponding electronic Stark tuning rate $\Delta\boldsymbol{\mu}_{eg}$ will change with the waiting time T, which in turn makes the dyadic product become a function of T. If any of these processes induce such changes in not only the magnitude of $\Delta\boldsymbol{\mu}_{eg}$ but also the relative angle between the two Stark tuning rates, then the sign of CLS could change too. Sign changes in the CLS have, in fact, been observed in several systems.[19,29,21] Therefore, the measurement of the CLS can provide not only the solvent correlation function, e.g., solvation dynamics or time-correlation function of the solvent electric field, but also molecular processes that affect the molecular structure via chemical reactions or conformational transitions.

The short-range Coulomb interaction between chromophores and surrounding solvent molecules could not be

https://dx.doi.org/10.1021/acs.jpcb.0c08959
J. Phys. Chem. B 2020, 124, 11222−11235

accurately described by the dipole−electric-field interaction. Considering both a set of distributed partial charges and the solvent electric potentials at the sites, the difference Coulomb interaction energy can be written as

$$\delta V_{eg}(\mathbf{q}) = -\sum_{j=1}^{n} (q_j^e - q_j^g)\, \phi_{\text{solvent}}(\mathbf{r}_j, \mathbf{q}) = -\sum_{j=1}^{n} \Delta q_j\, \phi_{\text{solvent}}(\mathbf{r}_j, \mathbf{q}) \tag{54}$$

where q_j^e and q_j^e represent the atomic or distributed partial charges of the jth site in the electronically excited and ground states, respectively. The number of distributed sites is n. Δq_j has been referred to as the transition charge of the jth site, which reflects the change in the electronic structure upon an electronic transition. $\mathbf{r}_j$ is the position of the chromophore's jth site. $\phi_{\text{solvent}}(\mathbf{r}_j, \mathbf{q})$ is the solvent electric potential at the chromophores' jth site, which is given as

$$\phi_{\text{solvent}}(\mathbf{r}_j, \mathbf{q}) = \frac{1}{4\pi\varepsilon} \sum_{k=1}^{M} \sum_{l=1}^{m} \frac{c_{kl}}{|\mathbf{r}_j - \mathbf{R}_{kl}|} \tag{55}$$

where ε is the dielectric constant of the medium, k is the index representing each solvent molecule, l is the index representing each atomic site of a given solvent molecule, c_{kl} is the atomic partial charge of the lth atom of the kth solvent molecule, and $\mathbf{R}_{kl}$ is the position of the atomic site of the lth atom of the kth solvent molecule. The number of solvent molecules is M, and the number of atoms in a given solvent molecule is m.

With the Coulomb interaction in eq 54, the fluctuating parts of the vibrational frequencies are[15,40,45]

$$\delta\hat{F}_g V_g(\mathbf{q}) = -\sum_{j=1}^{n} (\hat{F}_g q_j^g)\, \phi_{\text{solvent}}(\mathbf{r}_j, \mathbf{q}) = -\sum_{j=1}^{n} l_j^g\, \phi_{\text{solvent}}(\mathbf{r}_j, \mathbf{q})$$

$$\delta\hat{F}_e V_e(\mathbf{q}) = -\sum_{j=1}^{n} (\hat{F}_e q_j^e)\, \phi_{\text{solvent}}(\mathbf{r}_j, \mathbf{q}) = -\sum_{j=1}^{n} l_j^e\, \phi_{\text{solvent}}(\mathbf{r}_j, \mathbf{q}) \tag{56}$$

In eq 56, $l_j^{g/e}$ is known as the vibrational solvatochromic charge of the jth site, which is a measure of the susceptibility of the vibrational frequency in response to a small change in the local solvent electric potential at the jth site of the chromophore.

From eqs 54 and 56, one can write the cross FFCFs that determine the line shape of the 2DEV spectrum as

$$\langle \delta\omega_{eg}(T)\, \delta\omega_{g'g}(0)\rangle = \frac{1}{\hbar^2} \sum_{j=1}^{n} \sum_{j'=1}^{n} \langle \Delta q_j l_{j'}^g\, \phi_{\text{solvent}}(\mathbf{r}_j, \mathbf{q}(T))\, \phi_{\text{solvent}}(\mathbf{r}_{j'}, \mathbf{q}(0))\rangle_c$$

$$\langle \delta\omega_{eg}(T)\, \delta\omega_{e'e}(0)\rangle = \frac{1}{\hbar^2} \sum_{j=1}^{n} \sum_{j'=1}^{n} \langle \Delta q_j l_{j'}^e\, \phi_{\text{solvent}}(\mathbf{r}_j, \mathbf{q}(T))\, \phi_{\text{solvent}}(\mathbf{r}_{j'}, \mathbf{q}(0))\rangle_c \tag{57}$$

The result in eq 57 suggests that the magnitude and sign of the cross FFCFs are determined by the products of electronic transition charges and vibrational solvatochromic charges. The decays of the FFCFs are described by the weighted sums of the time-correlation functions of solvent electric potentials at different interaction sites.

Although the interaction between the distributed charges of a given chromophore and the electric field produced by surrounding solvent molecules is often the dominant contribution to the total intermolecular interaction potential of chromophores in polar solvents, the vibrational solvatochromism was found to be complicated due to non-negligible contributions from other interaction terms like exchange-repulsive, induction, and dispersion interactions.[16,42,46−48] Such difficulty in quantitatively describing the vibrational frequency shift induced by chromophore−solvent interaction is mainly because the vibrational frequency shift results from a variety of short-range interactions of a given localized vibrational mode with solvent molecules near the chromophore. Therefore, to estimate the cross FFCFs quantitatively, one might need to use other sophisticated approaches that were reviewed in ref 18.

CONCLUSIONS

2DEVS is a hybrid 2D spectroscopic technique utilizing IR and visible (or near-IR) pulses to excite chromophores electronically and subsequently to probe changes in their vibrational structures. We developed a theory of 2DEVS, which reveals the relationships between solvation dynamics of an electronically excited molecule and vibrational solvatochromism of vibronically coupled modes in the electronically excited and ground states. The CLS of each 2DEV peak is shown to be related to the cross-correlation between the fluctuating parts of the electronic and vibrational energy gaps. As an example, considering a simple electric Stark effect on the frequency shift originating from the interaction between solvent electric field and dipole moment of the chromophore, we showed that the solvent electric field−field correlation function weighted by the dyadic product of the electronic and vibrational Stark tuning rates determines the time-dependent change of the center line slope (CLS) of a given 2DEVS spectrum. However, the theoretical expressions given in the present work are general enough to describe the line shapes of the 2DEV spectra that are determined by a variety of molecular properties such as the vibronic coupling strengths, the initial amplitudes and signs of the cross FFCFs, the inhomogeneous distributions of electronic, vibrational, and vibronic frequencies, potential anharmonicities of vibronically coupled modes in the electronically excited states, the time scales of solvation dynamics, the correlation time of the vibrational solvatochromic frequency fluctuation, chemical reactions, and so on. Therefore, 2DEVS could be an incisive technique that would be of great use in studying photochemical reactions and the effects of solvent dynamics on the vibrational structures of such chemically and biologically reactive molecules in the condensed phases.

AUTHOR INFORMATION

Corresponding Author

Minhaeng Cho − *Center for Molecular Spectroscopy and Dynamics, Institute for Basic Science, Seoul 02841, Republic of Korea; Department of Chemistry, Korea University, Seoul*

https://dx.doi.org/10.1021/acs.jpcb.0c08959
J. Phys. Chem. B 2020, 124, 11222−11235

02841, Republic of Korea; orcid.org/0000-0003-1618-1056; Email: mcho@korea.ac.kr

Author

Graham R. Fleming − *Department of Chemistry, University of California, Berkeley, California 94720, United States; Molecular Biophysics and Integrated Bioimaging Division, Lawrence Berkeley National Laboratory, Berkeley, California 94720, United States; Kavli Energy NanoSciences Institute at Berkeley, Berkeley, California 94720, United States;* orcid.org/0000-0003-0847-1838

Complete contact information is available at: https://pubs.acs.org/10.1021/acs.jpcb.0c08959

Notes

The authors declare no competing financial interest.

■ ACKNOWLEDGMENTS

We thank Taka for his close friendship with us over the past three decades and for allowing us to enjoy his extraordinary sense of humor, not to mention his scientific insights and stimulating discussion. This work was supported by the Institute for Basic Science (IBS-R023-D1) (M.C.) and by the U.S. Department of Energy, Office of Science, Basic Energy Sciences, Division of Chemical Sciences, Geosciences and Biosciences (G.R.F.). G.R.F. thanks Eric Arsenault for important discussions.

■ REFERENCES

(1) Mukamel, S. *Principles of Nonlinear Optical Spectroscopy*; Oxford University Press: Oxford, 1995.
(2) Cho, M. *Two-Dimensional Optical Spectroscopy*; CRC Press: Boca Raton, FL, 2009.
(3) Cho, M. Coherent Two-dimensional Optical Spectroscopy. *Chem. Rev.* **2008**, *108*, 1331−1418.
(4) Cho, M.; Vaswani, H. M.; Brixner, T.; Stenger, J.; Fleming, G. R. Exciton Analysis in 2D Electronic Spectroscopy. *J. Phys. Chem. B* **2005**, *109*, 10542−10556.
(5) Mukamel, S. Multidimensional Femtosecond Correlation Spectroscopies of Electronic and Vibrational Excitations. *Annu. Rev. Phys. Chem.* **2000**, *51*, 691−729.
(6) Jonas, D. M. Two-Dimensional Femtosecond Spectroscopy. *Annu. Rev. Phys. Chem.* **2003**, *54*, 425−463.
(7) Cho, M.; Brixner, T.; Stiopkin, I.; Vaswani, H.; Fleming, G. R. Two Dimensional Electronic Spectroscopy of Molecular Complexes. *J. Chin. Chem. Soc.* **2006**, *53*, 15−24.
(8) Hamm, P.; Lim, M.; Hochstrasser, R. M. Structure of the Amide I Band of Peptides Measured by Femtosecond Nonlinear-Infrared Spectroscopy. *J. Phys. Chem. B* **1998**, *102*, 6123−6138.
(9) Tanimura, Y.; Mukamel, S. Two-dimensional Femtosecond Vibrational Spectroscopy of Liquids. *J. Chem. Phys.* **1993**, *99*, 9496−9511.
(10) Hamm, P.; Zanni, M. T.: *Concepts and Methods of 2D Infrared Spectroscopy*; Cambridge University Press: Cambridge, 2011.
(11) Cho, M., Ed. *Coherent Multidimensional Spectroscopy*; Springer Nature: Singapore, 2019.
(12) Fayer, M. D., Ed. *Ultrafast Infrared Vibrational Spectroscopy*; CRC Press: Boca Raton, FL, 2013.
(13) Ganim, Z.; Chung, H. S.; Smith, A. W.; DeFlores, L. P.; Jones, K. C.; Tokmakoff, A. Amide I Two-Dimensional Infrared Spectroscopy of Proteins. *Acc. Chem. Res.* **2008**, *41*, 432−441.
(14) Roberts, S. T.; Ramasesha, K.; Tokmakoff, A. Structural Rearrangements in Water Viewed Through Two-Dimensional Infrared Spectroscopy. *Acc. Chem. Res.* **2009**, *42*, 1239−1249.
(15) Kim, H.; Cho, M. Infrared Probes for Studying the Structure and Dynamics of Biomolecules. *Chem. Rev.* **2013**, *113*, 5817−5847.
(16) Baiz, C. R.; Blasiak, B.; Bredenbeck, J.; Cho, M.; Choi, J. H.; Corcelli, S. A.; Dijkstra, A. G.; Feng, C. J.; Garrett-Roe, S.; Ge, N. H.; Hanson-Heine, M. W. D.; Hirst, J. D.; Jansen, T. L. C.; Kwac, K.; Kubarych, K. J.; Londergan, C. H.; Maekawa, H.; Reppert, M.; Saito, S.; Roy, S.; Skinner, J. L.; Stock, G.; Straub, J. E.; Thielges, M. C.; Tominaga, K.; Tokmakoff, A.; Torii, H.; Wang, L.; Webb, L. J.; Zanni, M. T. Vibrational Spectroscopic Map, Vibrational Spectroscopy, and Intermolecular Interaction. *Chem. Rev.* **2020**, *120*, 7152−7218.
(17) Oliver, T. A. A.; Lewis, N. H. C.; Fleming, G. R. Correlating the motion of electrons and nuclei with two-dimensional electronic-vibrational spectroscopy. *Proc. Natl. Acad. Sci. U. S. A.* **2014**, *111*, 10061−10066.
(18) Dong, H.; Lewis, N. H. C.; Oliver, T. A. A.; Fleming, G. R. Determining the Static Electronic and Vibrational Energy Correlations via Two-dimensional Electronic-vibrational Spectroscopy. *J. Chem. Phys.* **2015**, *142*, 174201.
(19) Gaynor, J. D.; Petrone, A.; Li, X. S.; Khalil, M. Mapping Vibronic Couplings in a Solar Cell Dye with Polarization Selective Two-Dimensional Electronic-Vibrational Spectroscopy. *J. Phys. Chem. Lett.* **2018**, *9*, 6289−6295.
(20) Gaynor, J. D.; Khalil, M. Signatures of Vibronic Coupling in Two-dimensional Electronic-vibrational and Vibrational-electronic Spectroscopies. *J. Chem. Phys.* **2017**, *147*, 094202.
(21) Oliver, T. A. A.; Fleming, G. R. Following Coupled Electronic-nuclear Motion through Conical Intersections in the Ultrafast Relaxation of beta-Apo-8 ʻ-carotenal. *J. Phys. Chem. B* **2015**, *119*, 11428−11441.
(22) Wu, E. C.; Ge, Q. H.; Arsenault, E. A.; Lewis, N. H. C.; Gruenke, N. L.; Head-Gordon, M. J.; Fleming, G. R. Two-dimensional Electronic-vibrational Spectroscopic Study of Conical Intersection Dynamics: An Experimental and Electronic Structure Study. *Phys. Chem. Chem. Phys.* **2019**, *21*, 14153−14163.
(23) Roy, P. P.; Shee, J.; Arsenault, E. A.; Yoneda, Y.; Feuling, K.; Head-Gordon, M.; Fleming, G. R. Solvent Mediated Excited State Proton Transfer in Indigo Carmine. *J. Phys. Chem. Lett.* **2020**, *11*, 4156−4162.
(24) Kwac, K.; Cho, M. Two-Color Pump-Probe Spectroscopies of Two- and Three-Level Systems: 2-Dimensional Line Shapes and Solvation Dynamics. *J. Phys. Chem. A* **2003**, *107*, 5903−5912.
(25) Arsenault, E. A.; Yoneda, Y.; Iwai, M.; Niyogi, K. K.; Fleming, G. R. Vibronic Mixing Enables Ultrafast Energy Flow in Light-harvesting Complex II. *Nat. Commun.* **2020**, *11*, 1460.
(26) Bhattacharyya, P.; Fleming, G. R. The Role of Resonant Nuclear Modes in Vibrationally Assisted Energy Transport: The LHCII Complex. *J. Chem. Phys.* **2020**, *153*, 044119.
(27) Cho, M. Nonlinear Response Functions for the Three-dimensional Spectroscopies. *J. Chem. Phys.* **2001**, *115*, 4424.
(28) Sung, J. Y.; Silbey, R. J. Four Wave Mixing Spectroscopy for a Multilevel System. *J. Chem. Phys.* **2001**, *115*, 9266−9287.
(29) Tanimura, Y.; Ishizaki, A. Modeling, Calculating, and Analyzing Multidimensional Vibrational Spectroscopies. *Acc. Chem. Res.* **2009**, *42*, 1270−1279.
(30) Jansen, T. L. C.; Saito, S.; Jeon, J.; Cho, M. Theory of Coherent Two-dimensional Vibrational Spectroscopy. *J. Chem. Phys.* **2019**, *150*, 100901.
(31) Fleming, G. R.; Cho, M. Chromophore-solvent Dynamics. *Annu. Rev. Phys. Chem.* **1996**, *47*, 109−134.
(32) Cho, M.; Yu, J.-Y.; Joo, T.; Nagasawa, Y.; Passino, S. A.; Fleming, G. R. The Integrated Photon Echo and Solvation Dynamics. *J. Phys. Chem.* **1996**, *100*, 11944−11953.
(33) de Boeij, W.; Pshenichnikov, M. S.; Wiersma, D. A. On the Relation Between the Echo Peak Shift and Brownian Oscillator Correlation Function. *Chem. Phys. Lett.* **1996**, *253*, 53−60.
(34) Fuller, F. D.; Ogilvie, J. P. Experimental Implementations of Two-Dimensional Fourier Transform Electronic Spectroscopy. *Annu. Rev. Phys. Chem.* **2015**, *66*, 667−690.
(35) Myers, J. A.; Lewis, K. L. M.; Tekavec, P. F.; Ogilvie, J. P. Two-color two-dimensional Fourier transform electronic spectroscopy with a pulse-shaper. *Opt. Express* **2008**, *16*, 17420−17428.

(36) Lepetit, L.; Cheriaux, G.; Joffre, M. Linear Techniques of Phase Measurement by Femtosecond Spectral Interferometry for Applications in Spectroscopy. *J. Opt. Soc. Am. B* **1995**, *12*, 2467−2474.
(37) Lepetit, L.; Joffre, M. Two-dimensional Nonlinear Optics Using Fourier-transform Spectral Interferometry. *Opt. Lett.* **1996**, *21*, 564−566.
(38) Cina, J. A.; Kiessling, A. J. Nuclear Wave-packet Dynamics in Two-dimensional Interferograms of Excitation-transfer Systems. In *Coherent Multidimensional Spectroscopy*; Cho, M., Ed.; Spring Nature: Singapore, 2019; pp 51−85.
(39) Bhattacharyya, P.; Fleming, G. R. Two-Dimensional Electronic-Vibrational Spectroscopy of Coupled Molecular Complexes: A Near-Analytical Approach. *J. Phys. Chem. Lett.* **2019**, *10*, 2081−2089.
(40) Cho, M. Correlation between Electronic and Molecular Structure Distortions and Vibrational Properties. I. Adiabatic Approximations. *J. Chem. Phys.* **2003**, *118*, 3480−3490.
(41) Cho, M. Vibrational Solvatochromism and Electrochromism: Coarse-grained Models and Their Relationships. *J. Chem. Phys.* **2009**, *130*, 094505.
(42) Błasiak, B.; Londergan, C. H.; Webb, L. J.; Cho, M. Vibrational Probes: From Small Molecule Solvatochromism Theory and Experiments to Applications in Complex Systems. *Acc. Chem. Res.* **2017**, *50*, 968−976.
(43) Bublitz, G. U.; Boxer, S. G. Stark Spectroscopy: Applications in Chemistry, Biology, and Materials Science. *Annu. Rev. Phys. Chem.* **1997**, *48*, 213−242.
(44) Fried, S. D.; Boxer, S. G. Measuring Electric Fields and Noncovalent Interactions Using the Vibrational Stark Effect. *Acc. Chem. Res.* **2015**, *48*, 998−1006.
(45) Kwac, K.; Cho, M. Molecular Dynamics Simulation Study of N-methylacetamide in Water. I. Amide I Mode Frequency Fluctuation. *J. Chem. Phys.* **2003**, *119*, 2247−2255.
(46) Błasiak, B.; Cho, M. Vibrational Solvatochromism. II. A First-principle Theory of Solvation-induced Vibrational Frequency Shift Based on Effective Fragment Potential Method. *J. Chem. Phys.* **2014**, *140*, 164107.
(47) Błasiak, B.; Cho, M. Vibrational Solvatochromism. III. Rigorous Treatment of the Dispersion Interaction Contribution. *J. Chem. Phys.* **2015**, *143*, 164111.
(48) Błasiak, B.; Ritchie, A. W.; Webb, L. J.; Cho, M. Vibrational Solvatochromism of Nitrile Infrared Probes: Beyond the Vibrational Stark Dipole Approach. *Phys. Chem. Chem. Phys.* **2016**, *18*, 18094−18111.

https://dx.doi.org/10.1021/acs.jpcb.0c08959
J. Phys. Chem. B 2020, 124, 11222−11235